Identification of cyclic-di-GMP-modulating protein residues by bi-directionally evolving a social trait in *Pseudomonas fluorescens*

Collin Kessler[1] and Wook Kim[1*]

[1] Department of Biological Sciences, Duquesne University, Pittsburgh, Pennsylvania, United States of America

* Corresponding author

Email: kimw1@duq.edu

Abstract

Modulation of the intracellular cyclic di-guanosine monophosphate (c-di-GMP) pool is central to the formation of structured bacterial communities. Genome annotations predict the presence of dozens of conserved c-di-GMP catalytic enzymes in many bacterial species, but the functionality and regulatory control of the vast majority remain underexplored. Here, we begin to fill this gap by utilizing an experimental evolution system in *Pseudomonas fluorescens* Pf0-1, which repeatedly produces a unique social trait through bidirectional transitions between two distinct phenotypes converging on c-di-GMP modulation. Parallel evolution of 33 lineages captured 147 unique mutations among 191 evolved isolates in genes that are empirically demonstrated, bioinformatically predicted, or previously unknown to impact the intracellular pool of c-di-GMP. Quantitative chemistry confirmed that each mutation causing the phenotypic shift predictably amplifies or reduces c-di-GMP production. We integrate our mutation, phenotype, and quantification data with current models of known regulatory and catalytic systems, describe a previously unknown relationship between a regulatory component of branched-chain amino acid biosynthesis and c-di-GMP production, and predict functions of unexpected proteins that clearly impact c-di-GMP production. Sequential mutations that continuously disrupt or recover c-di-GMP production across discrete functional elements suggest a complex and underappreciated interconnectivity within the c-di-GMP regulome of *P. fluorescens*.

Importance

Microbial communities comprise densely packed cells where competition for space and resources is fierce. In our model system, mutant cells with a dry (D) phenotype are selected from a population with a mucoid (M) phenotype, and vice versa, because M and D cells physically work together to spread away from the overcrowded colony. D cells produce high levels of c-di-GMP and M cells produce low levels, so each mutation impacts c-di-GMP production. C-di-GMP is a second

44 messenger which regulates diverse bacterial phenotypes that cause tremendous clinical and
45 environmental problems. Many bacteria possess dozens of enzymes that are predicted to produce c-di-
46 GMP, but most are considered to be non-functional. Here, we take advantage of the bi-directional
47 selection of M and D phenotypes to identify key residues that could force these enzymes to turn on or
48 off. Several unexpected proteins also participate in this process, but very little is known about them.
49

50 **Introduction**

51 Microbes utilize diverse signaling mechanisms to adapt and respond to a dynamic environment.
52 Cyclic di-guanosine monophosphate (c-di-GMP) is a ubiquitous secondary messenger in bacteria and
53 high intracellular levels of c-di-GMP characteristically repress flagellar motility while stimulating the
54 expression of biofilm-formation genes (1–4). Numerous c-di-GMP binding proteins and riboswitches
55 respond to intracellular levels of c-di-GMP to also regulate cellular morphology, virulence factors,
56 antibiotic production, and the cell cycle (5, 6). C-di-GMP is synthesized from two molecules of GTP by a
57 diguanylate cyclase (DGC) and hydrolyzed by a phosphodiesterase (PDE) (1). DGCs and PDEs are
58 identified by the GGDEF or EAL/HD-GYP domains, respectively, and there are also hybrid proteins with
59 both DGC and PDE functions (7, 8). *Pseudomonas* spp. typically possess greater than 50 predicted DGCs
60 or PDEs (9). Specific signaling pathways or regulators have been characterized to independently regulate
61 several DGCs and PDEs (10–17), and some have been demonstrated to be under allosteric control,
62 where a certain range of c-di-GMP levels either initiate or prevent enzymatic activity (18–22). However,
63 the function of the vast majority of bioinformatically predicted DGCs and PDEs have not been
64 empirically validated and their regulatory mechanisms remain unknown (23).

65 A previous experimental evolution study described the bidirectional evolution of mucoid (M)
66 and dry (D) colony phenotypes in *P. fluorescens* Pf0-1, which likely occurs through c-di-GMP oscillation
67 (24). An aging colony of M cells repeatedly produces spreading fans at the perimeter, which comprise

68 the original M cells along with new D mutant cells that produce a dry and wrinkly colony morphology on
69 their own. Additionally, an aging colony of D cells also repeatedly generates spreading fans, which
70 comprise the original D cells along with a new mutant that appears phenotypically identical to the
71 ancestral M. This bidirectional selection of M and D phenotypes occurs continuously because M and D
72 cells self-organize in space and physically work together to spread out from the nutrient-poor and
73 crowded conditions of dense colony growth, and neither type is capable of spreading out on their own.
74 Genetic analyses of five evolved isolates revealed characteristic mutations in *wsp* genes to suggest that
75 c-di-GMP production is likely elevated in D and reduced in M (24).
76 Here, we carry out a large-scale parallel evolution experiment using the bidirectional M-D
77 system to identify 147 unique genes that are empirically demonstrated, bioinformatically predicted, or
78 previously unknown to impact c-di-GMP levels. We expand the current model of c-di-GMP production by
79 the Wsp signal transduction system and identify unique missense mutations outside the conserved
80 catalytic domain of numerous DGCs that stimulate enzymatic activity. We also describe proteins with no
81 previous associations to c-di-GMP production that appear to influence the activity of several DGCs,
82 including a regulatory component of the branched-chain amino acid (BCAA) biosynthesis pathway.
83 Lastly, we map the interconnectivity of the c-di-GMP regulome through sequential mutations that
84 disrupt or recover c-di-GMP production across functionally discrete systems.
85
86 **Results and Discussion**
87 **Bidirectional evolution of mucoid and dry phenotypes occurs through intracellular c-di-GMP pool**
88 **oscillation**
89 The bidirectional selection of mucoid (M) and dry (D) phenotypes occurs continuously in our
90 experimental system (24) because neither type is capable of spreading out on their own, but a colony of
91 initially mixed M and D cells readily spreads out in a radial pattern without requiring additional

92 mutations (Fig. 1A). With the expectation that a large-scale utilization of this experimental evolution
93 system could identify diverse mechanisms of c-di-GMP modulation, we initially set up 25 parallelly
94 evolving lineages of M. As anticipated, we observed bidirectional transitions between M and D
95 phenotypes across all lineages. In total, we isolated over 600 strains, analyzed genome sequences of 191
96 strains, and quantified c-di-GMP in a subset of 56 strains. Remarkably, we detected a single mutation
97 associated with each phenotypic transition, with the exception of only few additional silent mutations
98 across all genome sequences (Fig. S1, Table S1, Table S1 – Source Data 1). Genome sequencing
99 successive strains within each lineage provided an internal control, which confirmed the exclusive
100 presence of the respective preceding mutations.

101 Among the 147 unique mutations detected, 81 mutations were in *wsp* genes and 66 mutations
102 were in other genes including those that are hypothetical. Motility assays showed that all D strains were
103 non-motile and all M strains were motile as expected, and LC-MS/MS quantification confirmed that c-di-
104 GMP was elevated in all D strains relative to their respective parent M strain (Table S1). Notably, many
105 mutations in non-*wsp* genes sequentially flanked specific mutations in the Wsp signal transduction
106 system, the most extensively studied c-di-GMP regulatory system in *Pseudomonas* spp. (17). Several
107 missense mutations observed in Wsp proteins identified in this study overlap with comparable
108 mutations from various *Pseudomonas* and *Burkholderia* studies that we had previously compiled from
109 the literature (17) (Fig. 2). However, the vast majority of our mutations had never been observed and
110 many occur outside functionally annotated domains. The data presented in Fig. 2 represent the most
111 comprehensive record of functionally important residues of the Wsp system to date and empower our
112 predictions of mutation consequences. We first focus on sequential mutations in the Wsp system to
113 reveal both predictable and surprising evolutionary innovations to modulate c-di-GMP production. For
114 the sake of an accessible narrative, we will primarily refer to five simplified lineages (Fig. 1B), with
115 corresponding c-di-GMP measurements (Fig. 1C) and colony morphologies (Fig. S2).

116

117 **Diverse mutations converge on the Wsp signal transduction system that dynamically rewire signal**

118 **flow to produce a spectrum of functional states**

119 The Wsp signal transduction system was first reported two decades ago in *P. fluorescens* (25)

120 and continues to serve as the primary model system of c-di-GMP regulation in pseudomonads. The Wsp

121 system comprises seven proteins encoded in a monocistronic operon under the control of an

122 unidentified transcriptional regulator (26), and the current functional model is based on a combination

123 of empirical studies and predictions based on homologies to the chemotaxis system in *Escherichia coli*

124 (17). The main difference with the latter is that the signal cascade is initiated by the extracellular sensory

125 domain of WspA detecting surface contact (27, 28) to ultimately drive c-di-GMP production by the DGC

126 WspR (Fig. 3). Given that a mutation in any one of the seven Wsp protein coding genes could potentially

127 increase or decrease c-di-GMP production through WspR, we expected *wsp* genes to be a common

128 target in our parallel evolution experiments. Indeed, the vast majority of the first transitions from the

129 ancestral M to D occurred through either a missense or an in-frame deletion mutation in *wsp* genes

130 (Table S1).

131 Across our subset of five lineages (Fig. 4), initial mutations appear to artificially activate WspA,

132 followed by surprisingly similar patterns of sequential mutations in various *wsp* genes to oscillate c-di-

133 GMP production. Lineages 2 and 3 began with the first respective D strain possessing a unique in-frame

134 deletion that partially spans the predicted methylation helices of WspA. Lineage 5 began with a

135 missense mutation in the phosphoreceiver domain of WspF (P105S), which likely disrupts its methyl-

136 esterase activity to keep WspA in an activated state. This activation is undone in the following M strain

137 by an in-frame deletion in *wspA* that removes the amino acid residue S329, then c-di-GMP production is

138 restored again in the next D strain through an in-frame deletion of residues 282-296 in WspA. This

139 deletion falls within the same deleted region as those observed in lineages 2 and 3 (Fig. 2, Fig. 4).

140 Although methylation of WspA remains to be empirically demonstrated, its predicted methylation
141 helices clearly have a functional role in Wsp signaling as they were commonly mutated to activate c-di-
142 GMP production (Fig. 2). Based on our mutation data and homologies to Tsr-methylation in the
143 chemotaxis system of *E. coli* (29), we predict that the residues Q285, E292, E299, Q502, and E512 are
144 methylated and the deletion of these sites mimics a methylated state. We also set up an independent
145 lineage to commence with an engineered *ΔwspC* M strain (Fig. 4, strain 1.0), under the expectation that
146 the deletion of *wspC* would steer downstream mutations away from the Wsp system. However, we
147 detected a missense mutation within the signaling domain of WspA (A381V) in the first D progeny strain
148 1.1, and the same A381V mutation was previously observed in an independently evolved D strain with
149 an unaltered *wspC* gene (24). We detected additional missense mutations in WspA's signaling domain to
150 independently stimulate c-di-GMP production (Fig. 2), which likely bypass the methylation requirement
151 to activate WspE.

152 Mutations that stimulate WspA were typically followed by a missense mutation in WspB, WspD,
153 or WspE (Table S1). A missense mutation in WspD (W90L) in lineage 2 reduced c-di-GMP production like
154 the WspB (L136P) mutation in lineage 1 (Fig. 4). The functional roles of WspB and WspD in signal relay
155 are loosely modeled after homology to CheW of *E. coli*, which remains as the least characterized protein
156 in the chemotaxis system. Mutations in CheW that successfully disrupt signal transduction are largely
157 limited to five unique amino acid clusters that situate on the protein surface and are essential for the
158 docking of CheW to Tsr (WspA homolog) (30). WspB and WspD also possess six and seven highly
159 conserved amino acid clusters, respectively (17). Our WspB L135P and WspD W90L mutations fall within
160 these conserved clusters that likely situate on the surface of WspB and WspD and natively act as docking
161 sites for WspA and WspE to permit signal relay. We also observed additional missense and in-frame
162 deletion mutations in WspB and WspD that independently impact c-di-GMP production (Fig.2, Table S1),

163 confirming that both WspB and WspD are necessary for Wsp signal transduction through domains and
164 interactions that remain to be characterized.

165 Loss-of-function mutations (i.e. nonsense and frameshift mutations) in *wspE* were exclusively
166 associated with D to M transitions throughout all lineages to reduce c-di-GMP production (Table S1).
167 These observations are not particularly surprising, since WspR cannot be phosphorylated in the absence
168 of a functional WspE (Fig. 3). In contrast, multiple missense and in-frame deletions were observed in the
169 phosphoreceiver domain of WspE to exclusively stimulate c-di-GMP production (Fig. 2). Accordingly,
170 mutations within the conserved phosphoreceiver domain of CheY, a WspE homolog in *Escherichia coli*,
171 can activate the protein without phosphorylation (31, 32). In addition, the DGC activity of WspR in *P.*
172 *aeruginosa* could be modulated in a phosphorylation-independent manner (16, 33). Artificial activation
173 of WspE would deregulate WspA-dependent activation, and was often the evolutionary solution to
174 recover c-di-GMP production when the upstream signaling components of the Wsp system became
175 functionally crippled (Table S1). The M strain 1.4 of lineage 1 carries a frameshift mutation in *wspE*,
176 which should terminally shut down the Wsp system, and the c-di-GMP level was reduced as predicted
177 (Fig. 4). However, c-di-GMP production was restored in this lineage once again in the following D strain
178 1.5 through a missense mutation in DgcH (V459G), a bioinformatically predicted DGC that impacts
179 biofilm formation in *P. aeruginosa* PAO1 (34). DgcH is not only capable of producing c-di-GMP, but at
180 one of the highest levels detected in our study (Fig. 4, Table S1). In contrast to the Wsp system, it is
181 difficult to predict functional consequences of mutations in other DGCs, since so little is known beyond
182 their conserved catalytic domain.

183

184 **Many DGCs are functionally capable of causing the M to D shift independently from WspR**

185 Sequential patterns of mutations and c-di-GMP quantification across all 33 lineages indicate that
186 the DGC DgcH is also a dominant contributor to the intracellular c-di-GMP pool under our experimental

187 conditions. Other known or predicted DGCs were typically targeted to modulate c-di-GMP levels after
188 the Wsp system and DgcH became genetically dysfunctional. One exception is MorA, which represents
189 the first mutation target in two lineages (Table S1). The first D strain 4.1 of lineage 4 carries an in-frame
190 deletion mutation in *dgcH* that removes amino acid residues 524-537 (Fig. 4, Fig. 5). Interestingly, the
191 GGDEF diguanylate cyclase domain of DgcH spans residues 537-693 and the removal of the immediately
192 adjacent residues appears to activate c-di-GMP production. We observed a reduction in c-di-GMP in the
193 following M strain 4.2, which has a missense mutation in DgcH (L634P). A search against NCBI's
194 conserved domain database identifies that the residues 619-643 contain the inhibitory I-site (22, 35),
195 with residue N637 as the predicted interaction site with c-di-GMP. Our mutation data supports this
196 annotation and the likelihood that DgcH is under allosteric control by c-di-GMP; the L634P mutation in
197 DgcH could mimic a c-di-GMP bound state to cause the observed reduction in c-di-GMP. We cannot
198 discount the possibility of additional regulatory mechanisms, since numerous missense and in-frame
199 deletion mutations were detected across the coding sequence of DgcH (Fig. 5). As already discussed
200 above, the V459G mutation greatly increased c-di-GMP production in lineage 1 (Fig. 4), and in lineage
201 27, the Q454P mutation caused a shift to the D phenotype then reverted back to the M phenotype
202 through another missense mutation (Q148P) (Table S1). Similar to DgcH, specific missense mutations in
203 other DGCs caused bi-directional shifts and most activating mutations were found outside their
204 conserved catalytic domain (Fig. 5). We also detected the I-site in other DGCs, with MorA being the lone
205 exception, but no associated mutations were observed (Fig. 5). To the best of our knowledge, no
206 functional studies have been carried out to characterize the bioinformatically predicted domains of
207 these DGCs beyond their catalytic domain. We have clearly established that our mutations impact c-di-
208 GMP production, which should stimulate future studies to characterize their catalytic and/or regulatory
209 consequences.
210

211 **Mutations in genes with previously unknown associations with c-di-GMP production integrate with**
212 **Wsp or other DGC mutations to modulate c-di-GMP levels**

213 We also observed mutations in bioinformatically annotated genes with no known associations
214 to c-di-GMP modulation, but with clear associations with Wsp components and other DGCs. This pattern
215 is best represented in lineage 5 (Fig. 4). Like most lineages, mutations initially accumulate within *wsp*
216 genes and deregulate the Wsp system. Subsequent strains D 5.5 and M 5.6 carry mutations that activate
217 then deactivate the DGC SadC, respectively. Surprisingly, strain 5.7 returns this lineage to the D
218 phenotype through a missense mutation in IlvH (G150S), which is predicted to function in the
219 biosynthesis of branched chain amino acids (BCAA). We observed three independent missense
220 mutations in IlvH across our study that exclusively cause a phenotypic shift from M to D and reduced
221 motility (Table S1). Accordingly, quantification of c-di-GMP shows that each of these three mutations
222 significantly increases c-di-GMP respective to their immediate M parent (Fig. 6). These results indicate
223 that a previously unknown relationship exists between BCAA biosynthesis and c-di-GMP production, and
224 we explore this relationship in detail below.

225 Lineage 5 returns to the M phenotype in strain 5.8 through a missense mutation in the
226 hypothetical protein Pfl01_0730 (D115N) (Fig. 4). This protein, hereon ParA (PAP2 associated c-di-GMP
227 regulator), shares homology with the PAP2 superfamily of proteins, suggesting that it may be involved in
228 phospholipid turnover and impact the bioavailability of phosphate within the cell (36). Although we
229 found the relative decrease in c-di-GMP in strain 5.8 to be not statistically significant from its parent
230 likely due to technical noise (Fig. 6), the observed mutation clearly drives the phenotypic transition from
231 D to M. Furthermore, if this mutation does not impact c-di-GMP levels, then we would not expect a
232 further transition through elevated c-di-GMP production. Indeed, we captured two independent
233 transitions back to the D phenotype, both with substantially increased c-di-GMP levels (Fig. 4). Strains
234 5.9a and 5.9b are sister strains that have developed unique chimeric Wsp proteins. Both chimeric

235 proteins (WspA::D and WspB::D) contain identical partial segments of WspD commencing at residue
236 158, situated immediately adjacent to the in-frame deletion detected in their common ancestral strain
237 5.4, which previously deactivated the Wsp system (Fig. 4). To determine whether or not these chimeric
238 proteins alone are sufficient to drive the phenotypic shift from M to D, we replaced the corresponding
239 native Wsp proteins in the ancestral M strain with each chimeric protein. In parallel, we also replaced
240 the corresponding naturally modified Wsp proteins in the immediate parental M strain 5.8 with each
241 chimeric protein. Both engineered strains in the ancestral M background retained the M phenotype, but
242 both engineered strains in the M strain 5.8 background recapitulated the D transition that was observed
243 in strains 5.9a and 5.9b (Table 1). These results indicate that the two chimeric Wsp proteins require
244 additional mutation(s) observed within this lineage to produce c-di-GMP. Both the WspA::D and
245 WspB::D chimeras have lost WspC, which is not surprising since the methylation sites of WspA were
246 removed previously in the D strain 5.3. Similarly, WspB is completely removed in the WspA::D chimera
247 and nearly 75% of WspB has been removed in the WspB::D chimera. At this stage, it remains unclear
248 whether or not the observed mutations in *ilvH* and/or *parA* are required for the function of the two Wsp
249 chimeras. However, we present additional evidence below that strengthens the relationship between
250 IlvH and the Wsp system.

251 The WspB::D chimera strain 5.9b was next used to evolve M progeny strains. Sister strains 5.10a
252 and 5.10b were isolated and each were found to carry frameshift deletions in *ilvI* that decreased c-di-
253 GMP levels (Fig. 4). The two *ilvI* mutants carry a deletion of 17 or 23 nucleotides that start at the same
254 position, which should abolish IlvI's function by causing a frameshift. IlvI and IlvH form a complex that
255 catalyzes the first step of BCAA biosynthesis, where IlvH serves as the regulatory subunit and IlvI serves
256 as the catalytic subunit (37). IlvH in *E. coli* has been bioinformatically predicted to respond to c-di-GMP
257 levels due to the presence of the inhibitory I-site (35), which we also detected in most DGCs (Fig. 5). We
258 identified that IlvH of *P. fluorescens* Pf0-1 also contains the I-site RXXD motif at residues 103-106. None

259 of the independently identified IlvH mutations (A36E, S149R, and G150S) in our study fall within this
260 motif, but all three mutations significantly increase c-di-GMP levels (Fig. 6). Beyond the potential
261 allosteric regulation of IlvH by c-di-GMP, there is no known relationship between BCAA biosynthesis and
262 c-di-GMP production to the best of our knowledge. However, we suspected that the IlvH mutations,
263 including the G150S mutation observed earlier in this lineage, increase BCAA production to stimulate c-
264 di-GMP production through an unknown mechanism, since we subsequently observed frameshift
265 mutations in the catalytic subunit (IlvI) that returns this lineage back to the M phenotype with reduced
266 c-di-GMP levels.

267 The frameshift mutations in *ilvI* should lead to BCAA auxotrophy, which is likely masked by the
268 nutrient-rich medium utilized in our experimental evolution system. To test this prediction, we grew
269 strains 5.10a and 5.10b in a chemically defined minimal medium without BCAA. We did not observe any
270 growth unless BCAA was exogenously supplemented (Fig. S3), confirming that our *ilvI* mutants are
271 unable to synthesize BCAA. We next tested if exogenous supplementation of BCAA alone could restore
272 c-di-GMP production in the *ilvI* mutant (M strain 5.10a). Since the *ilvI* mutant cannot grow in the
273 minimal medium without BCAA supplementation, we also included our prototype M and D ancestors
274 (Fig. 1A) as relative controls in addition to the *ilvH* mutant (D strain 5.7) and the *parA* mutant (M strain
275 5.8) from the same lineage. Exogenous supplementation of BCAA in the *ilvI* mutant indeed restored c-di-
276 GMP production at comparable levels to both D and the *ilvH* mutant (D strain 5.7) (Fig. 7). In contrast, c-
277 di-GMP levels remained the same in both M and the *parA* mutant (M strain 5.8) regardless of BCAA
278 supplementation (Fig. 7). These results show that overabundance of BCAA does not correlate with c-di-
279 GMP production and defeats our initial prediction that the missense mutations in *ilvH* increase BCAA
280 production to stimulate c-di-GMP production. Although BCAA supplementation restores c-di-GMP
281 production in the *ilvI* mutant strain in the minimal medium, the reduction of c-di-GMP levels observed in
282 the same *ilvI* mutant under our nutrient-rich experimental evolution conditions (Fig. 6) is not likely

283 associated with losing the ability to synthesize BCAA. Accordingly, reconstructing the two frameshift *ilvI*
284 mutations independently in the ancestral D strain did not cause a shift to the M phenotype, but the
285 initially observed shift to the M phenotype was recapitulated when these mutations were introduced
286 into their direct parental D strains (Table 1). Since IlvI forms a complex with IlvH, the observed
287 frameshift mutations in *ilvI* likely decouple the complex, and consequently impact IlvH's function to
288 modulate c-di-GMP production. Lineage five returns to the D phenotype in four sister branches
289 following the *ilvI* mutations through mutations in *wspE* or *dcgH* (Fig. 4). As already discussed above, we
290 commonly observed activating *wspE* mutations when the upstream signaling Wsp components are
291 disrupted, and the in-frame deletion in *dgcH* is also identical to the deletion reported in the D strain 4.1.
292 These four independent transition steps into the D phenotype clearly indicate that the catalytic activity
293 of IlvI is not required for c-di-GMP production.

294 Lineage 27 was commenced with an engineered *ΔwspCD* M strain (Table S1, strain 27.0), where
295 we also observed the shift to the D phenotype through a missense mutation in IlvH (A36E) by restoring
296 c-di-GMP production (Fig. 6). In contrast to the M-shifting ParA (D115N) mutation that followed the D-
297 shifting IlvH (G150S) mutation in lineage 5, the transition from IlvH (A36E) to the M phenotype was
298 associated with a mutation which converts the stop codon of *wspB* with a cysteine residue to extend its
299 open reading frame, but out of frame with *wspE* (both *wspC* and *wspD* were already deleted). A
300 common trend exists between lineages 5 (Fig. 4) and 27 (Table S1) in that multiple mutations first occur
301 in Wsp proteins, which is proceeded by mutations in a non-Wsp DGC (SadC or DgcH, respectively), then
302 unique missense mutations occur in IlvH to stimulate c-di-GMP production. Reconstructing the three
303 IlvH missense mutations in the ancestral M strain does not lead to a shift to the D phenotype, but
304 reconstructing these mutations in their direct parental M strain recapitulates the initially observed shift
305 to the D phenotype (Table 1). The common targets of mutations between the two lineages that
306 converge on IlvH mutations are Wsp proteins, which implies that the c-di-GMP stimulating mutations in

307 IlvH specifically associate with a de-regulated Wsp system. Furthermore, the undoing of the IlvH (A36E)-
308 induced c-di-GMP production by the stop codon mutation in *wspB* implies potential IlvH-Wsp
309 interactions that are unlikely to be purely metabolic in nature.
310
311 **A macro assessment of sequential mutation patterns across all 33 parallel lineages captures potential**
312 **associations within the c-di-GMP regulome**
313 A long-standing question in the field is why microbes possess so many independent DGC and/or
314 PDE machineries. A systematic analysis of genes that are bioinformatically predicted to be DGCs in *P.*
315 *fluorescens* demonstrated that most have little impact on the intracellular c-di-GMP pool (9), and a
316 significant number of DGCs/PDEs in *E. coli* are present in an inactive form (8). In addition, independent
317 DGCs could regulate a sub-cellularly localized role (38) that could also contribute to the total
318 intracellular pool to regulate diverse physiological pathways across a gradient (39). Our study indicates
319 that many known or predicted DGCs could be independently stimulated to trigger a common phenotypic
320 shift, which appears to operate across a broad range of c-di-GMP levels (Fig. 1C). We also captured
321 mutations in genes with unknown associations with c-di-GMP modulation that significantly impact the c-
322 di-GMP pool (Table S1). Repetitive patterns of sequential mutations across independently evolving
323 lineages could reveal previously unknown connectivity between discrete regulatory and catalytic
324 elements.
325 To visualize conserved patterns of mutations across our complex dataset, we compiled all
326 sequences of mutation events across the 33 parallel lineages into a single node-edge plot (40) (Fig. 8A).
327 The nodes represent the mutated genes in our experiment. The edges (i.e. lines) of the plot report if the
328 mutation causes an M (blue) or D (orange) phenotype, and the thickness of the edge reflects the
329 frequency of the observed pattern (Table S2). Proteins that are integrated into this plot – meaning that
330 many edges connect to a specific node – collectively form the main ring. Nodes associated with a single

331 edge fall out of this ring, and mutations in these proteins typically occur at the end of a lineage or a
332 branched sub-lineage that was not sequenced. Since we did not sequence any progeny strains from
333 these ten mutants that fall outside of the main ring, we will not discuss them further.

334 The largest nodes in Fig. 8A are represented by Wsp proteins, DgcH, and other known DGCs like
335 YfiN, GcbC, MorA, and SadC. The majority of DGCs have blue recursive edges that cause an M
336 phenotype, which indicates that mutations occur in the same protein to shut down its activity,
337 immediately following a mutation that initially stimulated its activity. The high frequency of blue
338 recursive edges associated with each DGC and yellow edges between distinct DGCs collectively indicate
339 that each DGC simply replaces another to restore c-di-GMP production. Blue edges between DGCs are
340 extremely rare, which suggests that individual DGCs do not directly interact with another. Notably, there
341 are several proteins with both yellow and blue edges that are integrated in this plot and have not been
342 shown to have a role in c-di-GMP regulation or production. We next infer potential function of these
343 proteins with respect to c-di-GMP modulation.

344 ***NarA*** (N-ethylammeline chlorohydrolase associated c-di-GMP regulator): Pfl01_3147 is
345 annotated as a hypothetical protein, but we found homology to an N-ethylammeline chlorohydrolase. In
346 strain 2.3, we observe that the A383S mutation in NarA increases c-di-GMP levels (Fig. 8B), which
347 confirms that this hypothetical protein is indeed biologically active. This NarA mutation follows the M-
348 shifted W90L mutation in WspD, which suggests that NarA is either able to restore Wsp signaling or
349 activate other DGCs to increase c-di-GMP levels. We have no reason to suspect that NarA directly
350 catalyzes c-di-GMP since it lacks any c-di-GMP associated domains or motifs. The progeny of this NarA
351 mutant carries a nonsense mutation in *wspD*, reverting this strain back to an M phenotype (Table S1).
352 Thus, the A383S mutation in NarA associates specifically with *wspD* mutations to both restore and shut
353 down c-di-GMP production. NarA is predicted to catalyze N-ethylammeline, a derivative of ammeline,
354 and a recent study theorized that ammeline is likely an essential building block required for the

355 synthesis of cyclic complexes (41). Although the metabolic connections are unknown, there is a strong
356 indication that NarA interacts with WspD at some capacity to modulate c-di-GMP levels.
357 ***CdrB*** (Two-partner secretion system transporter): Pfl01_0652 encodes a protein that shares
358 homology with the transporter protein CdrB in *P. aeruginosa* (PA4624). In *P. aeruginosa*, CdrA and CdrB
359 are encoded in a single operon and form a two-partner secretion (TPS) system associated with biofilm
360 formation (42). CdrA (c-di-GMP regulated TPS A) is an extracellular adhesin known to respond to
361 modifications made by the periplasmic protease LapG which is activated by the transmembrane c-di-
362 GMP receptor LapD (43). It has been reported that high intracellular levels of c-di-GMP enable CdrA to
363 bind and crosslink secreted Psl, thereby increasing cell-cell adhesion (42). *cdrA/B* expression also
364 increases proportionally with intracellular levels of c-di-GMP during biofilm formation (44). CdrB is a
365 transporter with domains that indicate it is a type V secretion system transporter. CdrB is likely involved
366 in the transport of the adhesin CdrA but has no identified role in c-di-GMP modulation. In our lineage 6,
367 the missense mutation YfiN (G157C) increases c-di-GMP production, which is immediately followed by
368 the CdrB A290T missense mutation to decrease c-di-GMP levels (Fig. 8B). This suggests that an unaltered
369 CdrB or its native transport activity is necessary for YfiN's DGC activity. Mutations that follow the CdrB
370 mutation occur in *morA* or *dgcH*, each increasing c-di-GMP as indicated by the D-phenotype (Table S1).
371 Therefore, the negative impact of our CdrB mutation on YfiN could be recovered through the genetic
372 activation of other DGCs, which could also reflect interactions with CdrB.
373 ***CalM*** (c-di-GMP associated LysM): The hypothetical gene Pfl01_1895, hereon *calM* (c-di-GMP
374 associated LysM) is a commonly mutated gene in our study (Table S1). The encoded protein contains
375 domains with homology to the LysM peptidoglycan-binding superfamily and contains a FimV C-terminal
376 transmembrane domain that is implicated in modulating motility (45, 46). The LysM proteins are
377 identified by the lysin motif which is associated with cell lysis. The presence of the LysM and FimV
378 domains suggests that this protein may respond to changes in peptidoglycan stress, which is essential

379 for maintaining cell shape and integrity. C-di-GMP is a well-known regulator of cellular morphology in
380 *Vibrio cholera* and *Caulobacter crescentus* (13, 47). In addition, surface-sensing through the Wsp system
381 in *P. aeruginosa* was recently demonstrated to be associated with cell envelope stress (28). We
382 observed a duplication of five nucleotides within *calM* that results in a significant decrease in c-di-GMP
383 (Fig. 8B). Two repetitive clusters of CAGCG shifts to three clusters to cause a frameshift. This mutation
384 follows a *dcgH* in-frame deletion that dramatically increases c-di-GMP production, indicating that CalM
385 is necessary for DgcH's activity. Remarkably, three independently evolved progeny strains in this lineage
386 carry mutations that remove the initial five nucleotide insertion, returning each strain back to the D
387 phenotype likely by restoring DgcH's activity (Table S1).
388 ***RndA*** (RND transporter): Pfl01_2749 is bioinformatically predicted to encode an RND
389 transporter. RND transporters function as efflux pumps to remove toxins, antibiotics, quorum sensing
390 (QS) molecules, and other metabolites (48). We observed that the nonsense mutation Q51* in
391 Pfl01_2749, hereon *rndA*, significantly decreases c-di-GMP levels (strain 11.2, Fig. 8B). A recent study
392 speculates that QS molecules contribute to a feedback loop to inhibit c-di-GMP production (49). Thus, an
393 active RndA could potentially modulate this feedback loop by expelling certain effector compounds to
394 stimulate c-di-GMP production. The *rndA* mutant shifts to the D phenotype through an in-frame deletion
395 that removes amino acid residues 524-537 in DgcH. This specific mutation was observed in multiple
396 lineages to exclusively stimulate c-di-GMP production.
397 ***DgcX* and *DgcY*** (Bioinformatically predicted DGCs): Pfl01_3550 and Pfl01_3508 are both
398 bioinformatically predicted to encode DGCs, but their enzymatic function has not yet been
399 demonstrated. Here, we establish that they are both functionally active in c-di-GMP catalysis and
400 annotate them as *dgcX* and *dgcY*, respectively, since genes *dgcA* through *dgcW* already exist.
401 Pfl01_3550, hereon *dgcX*, is a commonly mutated gene in our dataset which increases c-di-GMP (Table
402 S1). We observed a blue recursive loop in the node-edge plot for DgcX, which is consistent with other

403 known DGCs (Fig. 8A). We isolated two independently evolved D mutants with the same M350I
404 mutation, and an M mutant with an in-frame deletion of L289. Phenotypic and motility data support
405 that the observed mutations in *dgcX* influence the intracellular c-di-GMP pool. The genomic location of
406 *dgcY* is in a region of hypothetical genes that appear to form an operon. Interestingly, our *dgcY* mutant
407 strains carry large deletions of the hypothetical genes within this genomic region (Fig. 5). The deletion of
408 Pfl01_3505, Pfl01_3506, and the 5' UTR region of *dgcY* results in a significant increase in c-di-GMP
409 (Strain 6.5a, Fig. 8B), which likely replaces the native promoter region of *dgcY* with that of Pfl01_3505.
410 C-di-GMP is significantly decreased in the progeny strain 6.6a (Fig. 8B) after the deletion of Pfl01_3500-
411 Pfl01_3510, which includes *dgcY*. It is unclear whether or not the encoded proteins of the hypothetical
412 genes that flank *dgcY* are functionally related to DgcY. We had initially suspected that these hypothetical
413 genes could encode a complex signal transduction system like Wsp, but we did not detect any
414 homologous Wsp domains or other c-di-GMP associated motifs.
415 To confirm whether the observed mutations in these atypical c-di-GMP associated genes alone
416 could modulate c-di-GMP levels, we reconstructed representative mutations in their respective
417 ancestral backgrounds. None of the engineered strains produced a phenotypic shift, but reconstructing
418 the same mutations in their direct parental strains recapitulated the initially observed phenotypic shifts
419 (Table 1). These results clearly indicate that specific mutations in the associated DGCs are first required
420 to impact c-di-GMP levels. Although functional studies are required to prescribe specific mechanisms,
421 diverse cellular processes appear to be integrated with numerous catalytic machineries to modulate the
422 c-di-GMP pool in *P. fluorescens*, and the missense and in-frame deletion mutations observed in Wsp
423 proteins and other DGCs (Fig. 5) could reflect potential interaction sites.
424
425 **Conclusion**

426 Although we have extensive knowledge on how specific enzymes make or break c-di-GMP and
427 how this molecule interacts with a large number of regulatory elements to modulate diverse
428 physiological processes, relatively little is known about how C-di-GMP production itself is regulated. This
429 study takes advantage of a repeatedly evolving social trait in *P. fluorescens* to demonstrate how
430 numerous proteins could independently and collectively produce remarkable sequences of genetic
431 innovation to oscillate c-di-GMP levels. Our extensive library of functionally critical residues reinforces
432 the current model of the Wsp system, which heavily draws functional analogies to the *E. coli* chemotaxis
433 system and particularly lacks domain resolution in WspB and WspD. Beyond the Wsp system, we have
434 confirmed that several bioinformatically predicted DGCs are indeed enzymatically active and identified
435 unique missense and in-frame deletion mutations in multiple DGCs that fall outside their conserved
436 catalytic domain. These mutations likely reflect regulatory domains that are critical for modulating
437 enzymatic activity. We have also uncovered a set of unexpected or hypothetical proteins that clearly
438 have the capacity to influence c-di-GMP turnover. Three missense mutations in *ilvH* were identified to
439 independently stimulate c-di-GMP production, which appears to be independent of IlvH's primary role in
440 BCAA biosynthesis, but rather operates through an unknown interaction with the Wsp system. We have
441 identified the same I-site in IlvH as in most DGCs, which suggests that IlvH physically interacts with c-di-
442 GMP. Similarly, CdrB and RndA homologs in other organisms have been implicated to respond to c-di-
443 GMP levels, but they have never been associated with modulating c-di-GMP production. We have
444 confirmed that the mutations observed in these proteins alone do not impact c-di-GMP levels, but do so
445 specifically in the presence of genetically modified DGCS or the Wsp signal transduction system.
446 An emerging concept here is that the intracellular pool of c-di-GMP, whether it be subcellularly
447 localized or in sum, appears to be modulated through the catalytic activities of many independent DGCs
448 that are in tune with diverse proteins. Such intricacies are masked by the activities of DGCs with high
449 output, but they are clearly hardwired in the genome of *P. fluorescens* and reflect a complex and

450 underappreciated interconnectivity. Similar relationships could also manifest in other *Pseudomonas* and
451 related species that share the same DGCs and unexpected proteins described in this study. In particular,
452 very little is known about the functional domains of most DGCs beyond their conserved catalytic
453 domain. The vast majority of the missense mutations or in-frame deletions captured in this study occur
454 outside of the catalytic domain to clearly activate or shut down c-di-GMP production. Our extensive
455 library of functionally important mutations presented here should facilitate mechanistic studies of
456 phylogenetically conserved DGCs that remain heavily under-explored.
457

458 **Material and Methods**

459 **Strains and culture conditions**

460 All *Pseudomonas fluorescens* Pf0-1 (50) derivatives associated with parallel experimental
461 evolution are described in Table S1 and engineered strains are described in Table 1. Strains were
462 routinely grown in Lennox LB (Fisher BioReagents), *Pseudomonas* Minimal Medium (PMM) (51), or on
463 *Pseudomonas* Agar F (PAF) (Difco). *Pseudomonas* F (PF) broth (a non-agar variant of PAF) was prepared
464 with the following: pancreatic digest of casein 10 g/L (Remel), proteose peptone No. 3 10 g/L (Remel),
465 dipotassium phosphate 1.5 g/L (Sigma-Aldrich), and magnesium sulfate 1.5 g/L (Sigma-Aldrich). Cultures
466 were incubated at 30°C and shaken at 250 rpm when applicable.

467 **Parallel experimental evolution**

468 Pure cultures of the ancestral M strain or engineered M strains were grown overnight in 5mL LB
469 broth and 25uL volumes were spotted on PAF plates, then incubated at room temperature for 3 to 8
470 days to allow spreading fans to emerge. To ensure consistency across experiments, PAF plates were
471 always prepared and left to dry at room temperature for 2 days before being inoculated. One fan was
472 randomly sampled from each colony and streaked out on LB plates in duplicate. Sampling a fan always
473 produced two strains with either a mucoid (M) or dry (D) colony phenotype. A single isolated colony

474 exhibiting the D phenotype was randomly selected to start a new liquid culture and also frozen down.
475 This process was repeated to sample six independent fans (i.e. six lineages). Three of the six
476 independently isolated D strains were randomly selected and cultured as above to start the next round
477 of experimental evolution. We repeated the same sampling process as above except that new M
478 phenotypes were isolated instead. We bidirectionally selected M and D phenotypes for as many as 13
479 rounds for a single lineage, but the number of sampled fans at each step was reduced over time in a
480 varying manner across independent lineages. In total, approximately 600 independently evolved isolates
481 were frozen down across 33 parallel lineages. Every isolate was subjected to a motility assay in an LB
482 plate with 0.25% agar, and the prototype M and D ancestors were used as controls (24). In addition,
483 25uL of pure cultures of each isolate, the ancestral strain with the opposite phenotype, and a 1:1
484 mixture of both were spotted onto PAF plates in triplicate and assessed for cooperative radial spreading
485 (Fig. 1A) to filter out hyper-motile and non-cooperative mutants (24). Colony diameters were measured
486 and recorded after four days of incubation at room temperature and considered cooperative if the
487 measured diameter of the 1:1 colony exceeded both the diameters of the isolated mutant strain and the
488 respective ancestral strain. Isolates that failed this test were removed from this study.

489 **Reconstruction of naturally derived mutations in ancestral and direct parental backgrounds**

490 Experimentally evolved isolates were whole genome sequenced to identify the causal mutations
491 as described below. We reconstructed select naturally acquired mutations in the respective ancestral
492 background and also in the direct parental background using previously described methods (24). PCR
493 primers were developed from the sequence data to amplify mutations of interest and are reported in
494 Table S3. Isolates were grown overnight and underwent DNA extractions (Qiagen). Dream Taq DNA
495 Polymerase (ThermoFisher) was used in PCR reactions with purified DNA to generate insert fragments
496 carrying the mutations which ranged in size from 456bp to 934bp. PCR was carried out using the
497 recommended conditions of the Dream Taq amplification kit for amplicons below 2000bp. Inserts were

498 cloned into the pGEM-T Easy vector system (Promega) and then subcloned into the *Not*I site of the
499 suicide plasmid pSR47s (52). Suicide plasmids were heat shocked into *E. coli* S17.1λ*pir*, mated with the
500 target strains reported in Table S3 on LB plates at 30°C for 16 hours, then plated onto PMM plates
501 supplemented with 50 ug/ml kanamycin. We observed that *ilvI* mutants could not grow on PMM and
502 therefore replaced the PMM selection plate with an LB plate supplemented with 50 ug/ml kanamycin
503 and 100 ug/ml ampicillin for *ilvI* mutant constructs. Isolated colonies were grown overnight, serially
504 diluted and plated out on LB plates supplemented with 15% sucrose (w/v) for counterselection. Isolated
505 colonies were placed in cryo-storage as described above. Crude DNA extracts were made for each strain
506 where 100uL of overnight culture was boiled at 100°C, centrifuged at 15,000 RCF for 30 seconds, and
507 10uL of supernatant was used for PCR using the primers reported in Table S3. PCR products underwent
508 gel extraction and subsequent sanger sequencing (primers in Table S3) to confirm that the mutation was
509 successfully engineered into the target strain. Upon PCR confirmation, pure cultures of cells from cryo-
510 storage underwent DNA extraction (Qiagen) and were submitted for WGS which confirmed that no
511 additional mutations had accumulated in the target strains during mutant construction.

512 **DNA extraction, whole genome sequencing, and variant calling**

513 Pure cultures were grown overnight in 5mL LB broth at 30°C. 1 mL was spun down to form a
514 pellet for DNA extraction. Pelleted cells were mechanically lysed with the Qiagen TissueLyser LT at 50
515 oscillations/second for 10 minutes. The Qiagen DNeasy UltraClean Microbial DNA extraction kit was
516 used following the standard operating procedures. Samples were then eluted into 30uL H_2O after a 5
517 minutes incubation at 4°C with the elution media and stored at -20°C prior to shipment. Genomic DNA
518 library preparations were carried out by the Microbial Genome Sequencing Center (Pittsburgh, PA)
519 following standard operating procedures. Pooled and indexed samples were sequenced on the NextSeq
520 2000 platform and demultiplexed prior to data delivery. The Trimmomatic algorithm was used to group
521 and quality filter paired reads at a Phred score of 20 using a 4bp sliding window. The BreSeq algorithm

522 was used to align the paired reads to the *P. fluorescens* Pf0-1 reference genome (CP000094.2) and
523 evaluate for single nucleotide polymorphisms (SNPs), insertions, deletions, or rearrangements. Output
524 sequence data from BreSeq is compiled as 'Table S1 – Source Data 1' and was manually evaluated for
525 each strain to determine the order of mutations for a given lineage.

526 **Alignment of mutation data to annotated domains**

527 Domain analyses of Wsp proteins and DGCs were conducted and rendered as previously
528 described (17). Peptide sequences of the predicted or known DGCs were obtained from the
529 *Pseudomonas* Genome Database (53). NCBI's conserved domain database (CDD) was used to evaluate
530 the functional domains (54). Mutation data of Wsp proteins from this study were manually mapped to
531 the rendered consensus sequence of the respective Wsp protein (17).

532 **C-di-GMP extraction and LC-MS/MS**

533 An isolated colony of each strain was transferred to PF broth and grown overnight. Overnight
534 cultures were diluted to an OD_{600} of 0.04 in triplicate and incubated for 2-4 hours until the samples
535 reached an OD_{600} of 0.5, then promptly processed for c-di-GMP extraction. C-di-GMP extraction and
536 quantification procedures followed the protocols established by the Michigan State University Research
537 Technology Support Facility (MSU-RTSF): MSU_MSMC_009 protocol for di-nucleotide extractions and
538 MSU_MSMC_009a for LC-MS/MS, with the following modifications. All the steps of c-di-GMP extraction
539 were carried out at 4°C unless noted otherwise. 1mL of 0.5 OD_{600} culture was centrifuged at 15,000 RCF
540 for 30 seconds, and cell pellets were resuspended in 100uL of ice cold acetonitrile/methanol/water
541 (40:40:20 (v/v/v)) extraction buffer supplemented with a final concentration of 0.01% formic acid and
542 25nM c-di-GMP-Fluorinated internal standard (InvivoGen CAT: 1334145-18-4). Pelleted cells were
543 mechanically disturbed with the Qiagen TissueLyser LT at 50 oscillations/second for 2 minutes.
544 Resuspended slurries were incubated at -20°C for 20 minutes and pelleted at 15,000 RCF for 15 minutes
545 at 4°C. The supernatant was transferred to a pre-chilled tube then supplemented with 4uL of 15% w/v

546 ammonium bicarbonate (Sigma-Aldrich) buffer for stable cryo-storage. Extracts were stored at -80°C for
547 less than two weeks prior to LC-MS/MS analysis at MSU-RTSF. Sample degradation was observed with
548 repeated freeze-thaw cycles, so extracts were never thawed until LC-MS/MS analysis. All samples were
549 evaporated under vacuum (SpeedVac, no heat) and redissolved in 100uL mobile phase (10 mM TBA/15
550 mM acetic acid in water/methanol, 97:3 v/v, pH 5). LC-MS/MS quantification was carried out with the
551 Waters Xevo TQ-S instrument with the following settings: c-di-GMP-F at *m/z* transition of 693 to 346
552 with cone voltage of 108 and collision voltage of 33; c-di-GMP at *m/z* transition of 689 to 344 with cone
553 voltage of 83 and collision voltage of 31. C-di-GMP data was normalized to 25nM c-di-GMP-F by MSU-
554 RTSF to account for sample matrix effects and sample loss during preparation. OD_{600} measurements of
555 the initial samples were used to report the quantified c-di-GMP as nM/OD and visualized with GraphPad
556 Prism9.

557 **BCAA supplementation assay and c-di-GMP quantification**

558 Pure cultures were grown overnight in 5mL LB broth. 5uL of each culture was transferred into
559 5mL PMM. Cultures were supplemented with the BCAA valine, leucine, and isoleucine as previously
560 described (55). Assessment of growth during BCAA supplementation contained either 0uM (loading
561 control), 180uM, 200uM, 220uM, 250uM, or 300uM in triplicate. Samples were incubated at 30°C for 24
562 hours at 250 rpm shaking. Cultures were manually pipetted to resuspend cells and 300uL of culture was
563 transferred to a 96-well black wall clear bottom plate for OD_{600} quantification. OD was quantified using
564 the SpectraMax plate reader and background (determined from blanks) was removed from each
565 quantified sample. Data analysis and visualization of growth during BCAA supplementation was
566 conducted in Excel. To evaluate the relationship between BCAA and c-di-GMP, pure cultures were grown
567 for 24 hours at 30°C and 250 rpm shaking in PMM liquid media containing either 0uM, 50uM, 100uM or
568 150uM of supplemented BCAAs. OD_{600} measurements were taken and samples were diluted to an OD_{600}
569 of 0.04 into PMM at the same BCAA concentrations. Samples were incubated for 24 hours under the

570 same conditions stated and then sonicated (Time 0.00:20, Pulse 01 01, Amplitude 20%) to disrupt cell
571 aggregates. OD_{600} measurements occurred every hour until OD_{600} was approximately equal to 0.25. C-di-
572 GMP analyte extraction was carried out as stated above with the modification that 2mL cultures were
573 used for cell lysis. Quantified values of c-di-GMP are reported as nM/OD_{600} and were visualized with
574 GraphPad Prism9.

575 **Node-edge analysis and visualization**

576 Data reported in Table S1 was used to generate the 'to-from' table which assesses mutation
577 patterns at the gene/protein level (40). Counts were determined by the frequency of the to-from
578 patterns calculated from Table S1 where a mutation in a given gene/protein (to) occurred after a
579 mutation in another gene/protein (from). This table was uploaded to Cytoscape to visualize the nodes
580 (to genes/proteins) and edges (counts). Default renderings of the plot reported node centrality
581 (commonly mutated targets) through coordinate placement on the graph. This metric was converted to
582 node size with larger nodes representing more commonly mutated targets. Nodes were manually
583 aligned for visual clarity with nodes connected by two or more edges being placed in the main ring and
584 nodes with a single edge being placed outside the ring.

585

586 **Acknowledgments**

587 We thank RTSF (Michigan State University) for services and assistance with LC-MS/MS analyses and
588 MiGS (Pittsburgh, PA) for providing genome sequencing. This study was funded by the Charles Henry
589 Leach II Fund 217032 (W.K.) and the Faculty Development Fund G1700030 (W.K.) awarded by Duquesne
590 University.

591

592 **Author Contributions**

593 W.K. designed the study, C.K. performed the experiments, C.K and W.K analyzed data and wrote the
594 manuscript.
595
596 **Conflict of Interest**
597 The authors declare no conflict of interest.
598
599 **Table S1 – Source Data 1. BreSeq summary reports of mutations identified in strains isolated in this**
600 **study.** Whole genome sequencing data of select strains from the parallel evolution experiments were
601 subjected to variant analysis using the BreSeq algorithm against the published *P. fluorescens* Pf0-1
602 genome sequence. Summary files are provided for each analysis where the 'Strain ID' reported in Table
603 S1 is represented as the file name.
604
605 **References**

606 1. Römling U, Galperin MY, Gomelsky M. 2013. Cyclic di-GMP: the First 25 Years of a Universal
607 Bacterial Second Messenger. Microbiology and Molecular Biology Reviews 77:1–52.

608 2. Valentini M, Filloux A. 2016. Biofilms and Cyclic di-GMP (c-di-GMP) Signaling: Lessons from
609 *Pseudomonas aeruginosa* and Other Bacteria. Journal of Biological Chemistry 291:12547–12555.

610 3. Wolfe AJ, Visick KL. 2008. Get the message out: Cyclic-Di-GMP regulates multiple levels of
611 flagellum-based motility. Journal of Bacteriology https://doi.org/10.1128/JB.01418-07.

612 4. Jenal U, Reinders A, Lori C. 2017. Cyclic di-GMP: second messenger extraordinaire. Nature
613 Reviews Microbiology 15:271–284.

614 5. Tamayo R. 2019. Cyclic diguanylate riboswitches control bacterial pathogenesis mechanisms.
615 PLoS Pathogens 15.

616 6. Dahlstrom KM, Giglio KM, Sondermann H, O'Toolea GA. 2016. The inhibitory site of a diguanylate
617 cyclase is a necessary element for interaction and signaling with an effector protein. Journal of
618 Bacteriology 198:1595–1603.

619 7. Simm R, Morr M, Kader A, Nimtz M, Römling U. 2004. GGDEF and EAL domains inversely regulate
620 cyclic di-GMP levels and transition from sessility to motility. Molecular Microbiology 53:1123–
621 1134.

622 8. Hengge R, Galperin MY, Ghigo JM, Gomelsky M, Green J, Hughes KT, Jenal U, Landini P. 2016.
623 Systematic nomenclature for GGDEF and EAL domaincontaining cyclic di-GMP turnover proteins
624 of *Escherichia coli*. Journal of Bacteriology 198:7–11.

625 9. Newell PD, Yoshioka S, Hvorecny KL, Monds RD, O'Toole GA. 2011. Systematic Analysis of
626 Diguanylate Cyclases That Promote Biofilm Formation by *Pseudomonas fluorescens* Pf0-1. Journal
627 of Bacteriology 193:4685–4698.

628 10. Huertas-Rosales Ó, Romero M, Heeb S, Espinosa-Urgel M, Cámara M, Ramos-González MI. 2017.
629 The *Pseudomonas putida* CsrA/RsmA homologues negatively affect c-di-GMP pools and biofilm
630 formation through the GGDEF/EAL response regulator CfcR. Environmental Microbiology
631 19:3551–3566.

632 11. Merritt JH, Ha D-G, Cowles KN, Lu W, Morales DK, Rabinowitz J, Gitai Z, O'Toole GA. 2010.
633 Specific Control of *Pseudomonas aeruginosa* Surface-Associated Behaviors by Two c-di-GMP
634 Diguanylate Cyclases. mBio 1.

635 12. Ravichandran A, Ramachandran M, Suriyanarayanan T, Wong CC, Swarup S. 2015. Global
636 Regulator MorA Affects Virulence-Associated Protease Secretion in *Pseudomonas aeruginosa*
637 PAO1. PLOS ONE 10:e0123805.

638 13. Wassmann P, Chan C, Paul R, Beck A, Heerklotz H, Jenal U, Schirmer T. 2007. Structure of BeF3--
639 Modified Response Regulator PleD: Implications for Diguanylate Cyclase Activation, Catalysis, and
640 Feedback Inhibition. Structure https://doi.org/10.1016/j.str.2007.06.016.

641 14. Moscoso JA, Jaeger T, Valentini M, Hui K, Jenal U, Filloux A. 2014. The diguanylate cyclase SadC is
642 a central player in Gac/Rsm-mediated biofilm formation in *Pseudomonas aeruginosa*. Journal of
643 Bacteriology 196:4081–4088.

644 15. Giardina G, Paiardini A, Fernicola S, Franceschini S, Rinaldo S, Stelitano V, Cutruzzolà F. 2013.
645 Investigating the allosteric regulation of YfiN from *Pseudomonas aeruginosa*: Clues from the
646 structure of the catalytic domain. PLoS ONE 8.

647 16. De N, Pirruccello M, Krasteva PV, Bae N, Raghavan RV, Sondermann H. 2008. Phosphorylation-
648 Independent Regulation of the Diguanylate Cyclase WspR. PLoS Biology 6:e67.

649 17. Kessler C, Mhatre E, Cooper V, Kim W. 2021. Evolutionary divergence of the Wsp signal
650 transduction system in β- And γ-proteobacteria. Appl Environ Microbiol 87.

651 18. Mantoni F, Paiardini A, Brunotti P, D'Angelo C, Cervoni L, Paone A, Cappellacci L, Petrelli R,
652 Ricciutelli M, Leoni L, Rampioni G, Arcovito A, Rinaldo S, Cutruzzolà F, Giardina G. 2018. Insights
653 into the GTP-dependent allosteric control of c-di-GMP hydrolysis from the crystal structure of
654 PA0575 protein from *Pseudomonas aeruginosa*. FEBS Journal 285.

655 19. Giacalone D, Smith TJ, Collins AJ, Sondermann H, Koziol LJ, O'Toole GA. 2018. Ligand-mediated
656 biofilm formation via enhanced physical interaction between a diguanylate cyclase and its
657 receptor. mBio 9.

658 20. Christen B, Christen M, Paul R, Schmid F, Folcher M, Jenoe P, Meuwly M, Jenal U. 2006. Allosteric
659 Control of Cyclic di-GMP Signaling. Journal of Biological Chemistry 281:32015–32024.

660 21. Chan C, Paul R, Samoray D, Amiot N, Giese B, Jenal U, Schirmer T. 2005. Structural basis for the
661 activity and allosteric control of diguanylate cyclase. Acta Crystallographica Section A
662 Foundations of Crystallography https://doi.org/10.1107/s0108767305089993.

663 22. De N, Navarro MVAS, Raghavan R v., Sondermann H. 2009. Determinants for the Activation and
664 Autoinhibition of the Diguanylate Cyclase Response Regulator WspR. Journal of Molecular
665 Biology 393:619–633.

666 23. Dahlstrom KM, Collins AJ, Doing G, Taroni JN, Gauvin TJ, Greene CS, Hogan DA, O'Toole GA. 2018.
667 A multimodal strategy used by a large c-di-GMP network. Journal of Bacteriology 200.

668 24. Kim W, Levy SB, Foster KR. 2016. Rapid radiation in bacteria leads to a division of labour. Nature
669 Communications 7:10508.

670 25. Spiers AJ, Kahn SG, Bohannon J, Travisano M, Rainey PB. 2002. Adaptive divergence in
671 experimental populations of *Pseudomonas fluorescens*. I. Genetic and phenotypic bases of
672 wrinkly spreader fitness. Genetics 161:33–46.

673 26. Bantinaki E, Kassen R, Knight CG, Robinson Z, Spiers AJ, Rainey PB. 2007. Adaptive Divergence in
674 Experimental Populations of *Pseudomonas fluorescens*. III. Mutational Origins of Wrinkly
675 Spreader Diversity. Genetics 176:441–453.

676 27. Armbruster CR, Lee CK, Parker-Gilham J, de Anda J, Xia A, Zhao K, Murakami K, Tseng BS,
677 Hoffman LR, Jin F, Harwood CS, Wong GC, Parsek MR. 2019. Heterogeneity in surface sensing
678 suggests a division of labor in *Pseudomonas aeruginosa* populations. Elife 8:1–29.

679 28. O'neal L, Baraquet C, Suo Z, Dreifus JE, Peng Y, Raivio TL, Wozniak DJ, Harwood CS, Parsek MR.
680 2022. The Wsp system of *Pseudomonas aeruginosa* links surface sensing and cell envelope stress
681 https://doi.org/10.1073/pnas.

682 29. Rice MS, Dahlquist FW. 1991. Sites of deamidation and methylation in Tsr, a bacterial chemotaxis
683 sensory transducer. Journal of Biological Chemistry 266:9746–9753.

684 30. Li Y, Hu Y, Fu W, Xia B, Jin C. 2007. Solution structure of the bacterial chemotaxis adaptor protein
685 CheW from *Escherichia coli*. Biochemical and Biophysical Research Communications 360.

686 31. Re S da, Tolstykh T, Wolanin PM, Stock JB. 2002. Genetic analysis of response regulator activation
687 in bacterial chemotaxis suggests an intermolecular mechanism. Protein Science 11:2644–2654.

688 32. Bellsolell L, Prieto J, Serrano L, Coll M. 1994. Magnesium Binding to the Bacterial Chemotaxis
689 Protein CheY Results in Large Conformational Changes Involving its Functional Surface. Journal of
690 Molecular Biology 238:489–495.

691 33. Huangyutitham V, Güvener ZT, Harwood CS. 2013. Subcellular Clustering of the Phosphorylated
692 WspR Response Regulator Protein Stimulates Its Diguanylate Cyclase Activity. mBio 4:1–8.

693 34. Wei Q, Leclercq S, Bhasme P, Xu A, Zhu B, Zhang Y, Zhang M, Wang S, Maa LZ. 2019. Diguanylate
694 cyclases and phosphodiesterases required for basal-level c-di-GMP in *Pseudomonas aeruginosa*
695 as revealed by systematic phylogenetic and transcriptomic analyses. Applied and Environmental
696 Microbiology 85.

697 35. Fang X, Ahmad I, Blanka A, Schottkowski M, Cimdins A, Galperin MY, Römling U, Gomelsky M.
698 2014. GIL, a new c-di-GMP-binding protein domain involved in regulation of cellulose synthesis in
699 enterobacteria. Molecular Microbiology 93.

700 36. Carman GM, Han GS. 2006. Roles of phosphatidate phosphatase enzymes in lipid metabolism.
701 Trends in Biochemical Sciences https://doi.org/10.1016/j.tibs.2006.10.003.

702 37. Ricca E, Limauro D, Lago CT, de Felice M. 1988. Enhanced acetohydroxy acid synthase III activity
703 in an ilvH mutant of *Escherichia coli* K-12. J Bacteriol 170.

704 38. Massie JP, Reynolds EL, Koestler BJ, Cong J-P, Agostoni M, Waters CM. 2012. Quantification of
705 high-specificity cyclic diguanylate signaling. Proceedings of the National Academy of Sciences
706 109:12746–12751.

707 39. Yan J, Deforet M, Boyle KE, Rahman R, Liang R, Okegbe C, Dietrich LEP, Qiu W, Xavier JB. 2017.
708 Bow-tie signaling in c-di-GMP: Machine learning in a simple biochemical network. PLOS
709 Computational Biology 13:e1005677.

710 40. Shannon P, Markiel A, Ozier O, Baliga NS, Wang JT, Ramage D, Amin N, Schwikowski B, Ideker T.
711 2003. Cytoscape: A software Environment for integrated models of biomolecular interaction
712 networks. Genome Research 13.

713 41. Petelski AN, Fonseca Guerra C. 2019. Designing Self-Assembled Rosettes: Why Ammeline is a
714 Superior Building Block to Melamine. ChemistryOpen 8.

715 42. Reichhardt C, Wong C, da Silva DP, Wozniak DJ, Parsek MR. 2018. CDRA interactions within the
716 *Pseudomonas aeruginosa* biofilm matrix safeguard it from proteolysis and promote cellular
717 packing. mBio 9.

718 43. Cooley RB, Smith TJ, Leung W, Tierney V, Borlee BR, O'Toole GA, Sondermann H. 2016. Cyclic di-
719 GMP-regulated periplasmic proteolysis of a *Pseudomonas aeruginosa* type Vb secretion system
720 substrate. Journal of Bacteriology 198:66–76.

721 44. Borlee BR, Goldman AD, Murakami K, Samudrala R, Wozniak DJ, Parsek MR. 2010. *Pseudomonas*
722 *aeruginosa* uses a cyclic-di-GMP-regulated adhesin to reinforce the biofilm extracellular matrix.
723 Molecular Microbiology 75:827–842.

724 45. Wehbi H, Portillo E, Harvey H, Shimkoff AE, Scheurwater EM, Howell PL, Burrows LL. 2011. The
725 peptidoglycan-binding protein fimv promotes assembly of the *Pseudomonas aeruginosa* type IV
726 pilus secretin. Journal of Bacteriology 193.

727 46. Buendia L, Girardin A, Wang T, Cottret L, Lefebvre B. 2018. LysM receptor-like kinase and lysM
728 receptor-like protein families: An update on phylogeny and functional characterization. Frontiers
729 in Plant Science https://doi.org/10.3389/fpls.2018.01531.

730 47. Conner JG, Zamorano-Sánchez D, Park JH, Sondermann H, Yildiz FH. 2017. The ins and outs of
731 cyclic di-GMP signaling in Vibrio cholerae. Current Opinion in Microbiology 36:20–29.

732 48. Soto SM. 2013. Role of efflux pumps in the antibiotic resistance of bacteria embedded in a
733 biofilm. Virulence 4.

734 49. Liang F, Zhang B, Yang Q, Zhang Y, Zheng D, Zhang L, Yan Q, Wu X. 2020. Cyclic-di-GMP Regulates
735 the Quorum-Sensing System and Biocontrol Activity of *Pseudomonas fluorescens* 2P24 through
736 the RsmA and RsmE Proteins. Applied and Environmental Microbiology 86.

737 50. Compeau G, Al-Achi BJ, Platsouka E, Levy SB. 1988. Survival of rifampin-resistant mutants of
738 *Pseudomonas fluorescens* and *Pseudomonas putida* in soil systems. Applied and Environmental
739 Microbiology 54.

740 51. Kirner S, Krauss S, Sury G, Lam ST, Ligon JM, van Pée KH. 1996. The non-haem chloroperoxidase
741 from *Pseudomonas fluorescens* and its relationship to pyrrolnitrin biosynthesis. Microbiology (N
742 Y) 142.

743 52. Matthews M, Roy CR. 2000. Identification and subcellular localization of the *Legionella*
744 *pneumophila* IcmX protein: A factor essential for establishment of a replicative organelle in
745 eukaryotic host cells. Infection and Immunity 68.

746 53. Winsor GL, Griffiths EJ, Lo R, Dhillon BK, Shay JA, Brinkman FSL. 2016. Enhanced annotations and
747 features for comparing thousands of *Pseudomonas* genomes in the *Pseudomonas* genome
748 database. Nucleic Acids Research 44:D646–D653.

749 54. Lu S, Wang J, Chitsaz F, Derbyshire MK, Geer RC, Gonzales NR, Gwadz M, Hurwitz DI, Marchler
750 GH, Song JS, Thanki N, Yamashita RA, Yang M, Zhang D, Zheng C, Lanczycki CJ, Marchler-Bauer A.
751 2020. CDD/SPARCLE: the conserved domain database in 2020. Nucleic Acids Research 48:D265–
752 D268.

753 55. Kim W, Levy SB. 2008. Increased fitness of Pseudomonas fluorescens Pf0-1 leucine auxotrophs in
754 soil. Applied and Environmental Microbiology 74:3644–3651.

755 56. Feng X, Lilly AA, Hazelbauer GL. 1999. Enhanced Function Conferred on Low-Abundance
756 Chemoreceptor Trg by a Methyltransferase-Docking Site. Journal of Bacteriology 181:3164–3171.

757 57. Alexander RP, Lowenthal AC, Harshey RM, Ottemann KM. 2010. CheV: CheW-like coupling
758 proteins at the core of the chemotaxis signaling network. Trends in Microbiology 18:494–503.

759 58. Malone JG, Williams R, Christen M, Jenal U, Spiers AJ, Rainey PB. 2007. The structure–function
760 relationship of WspR, a *Pseudomonas fluorescens* response regulator with a GGDEF output
761 domain. Microbiology (N Y) 153:980–994.

762 59. O'Connor JR, Kuwada NJ, Huangyutitham V, Wiggins PA, Harwood CS. 2012. Surface sensing and
763 lateral subcellular localization of WspA, the receptor in a chemosensory-like system leading to c-
764 di-GMP production. Mol Microbiol 86:720–9.

765 60. Kim W, Racimo F, Schluter J, Levy SB, Foster KR. 2014. Importance of positioning for microbial
766 evolution. Proceedings of the National Academy of Sciences 111:E1639–E1647.

767

768

Figures and Tables

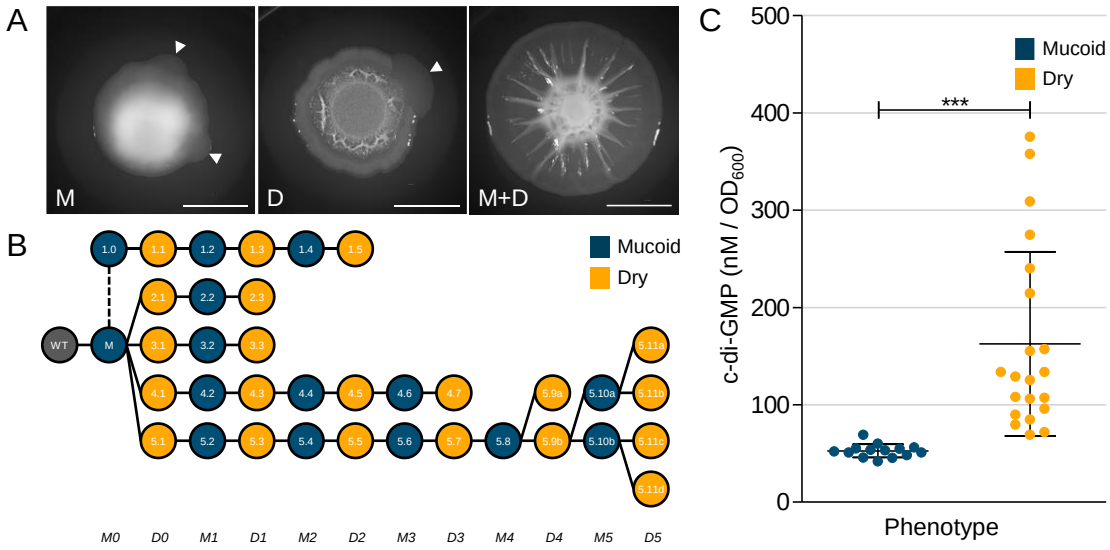

Figure 1. Bidirectional evolution of M and D phenotypes are c-di-GMP dependent. A) Colony morphologies of the ancestral mucoid (M, left) and dry (D, middle) strains after 4 days of growth. Arrows indicate the emergence of spreading fans that contain the respective parent strain and a new mutant strain with the opposite phenotype. The spreading phenotype is readily produced by artificially mixing M and D strains (right, scale bar = 10mm). B) Phylogeny of strains in select lineages colored by phenotype and corresponding colony morphologies are shown in Fig. S2. The numbers indicate the IDs of the evolved strains as shown in Table S1. Strain 1.0 was constructed from the ancestral M strain to lack the *wspC* gene, which encodes a methyltransferase known to activate the Wsp system. Each strain was isolated from naturally emerging fans from their respective parent colony with the opposite phenotype. This phylogeny depicts the bidirectional transitions between mucoid and dry states which we show are c-di-GMP dependent. C) C-di-GMP levels of evolved strains. C-di-GMP was quantified through LC-MS/MS and is reported as nM per OD600. Samples are categorized by phenotype and we report the triplicate mean ± SD for each phenotypic classification: mucoid n=14 and dry n=21 (*** Student's t-test $p < 0.001$).

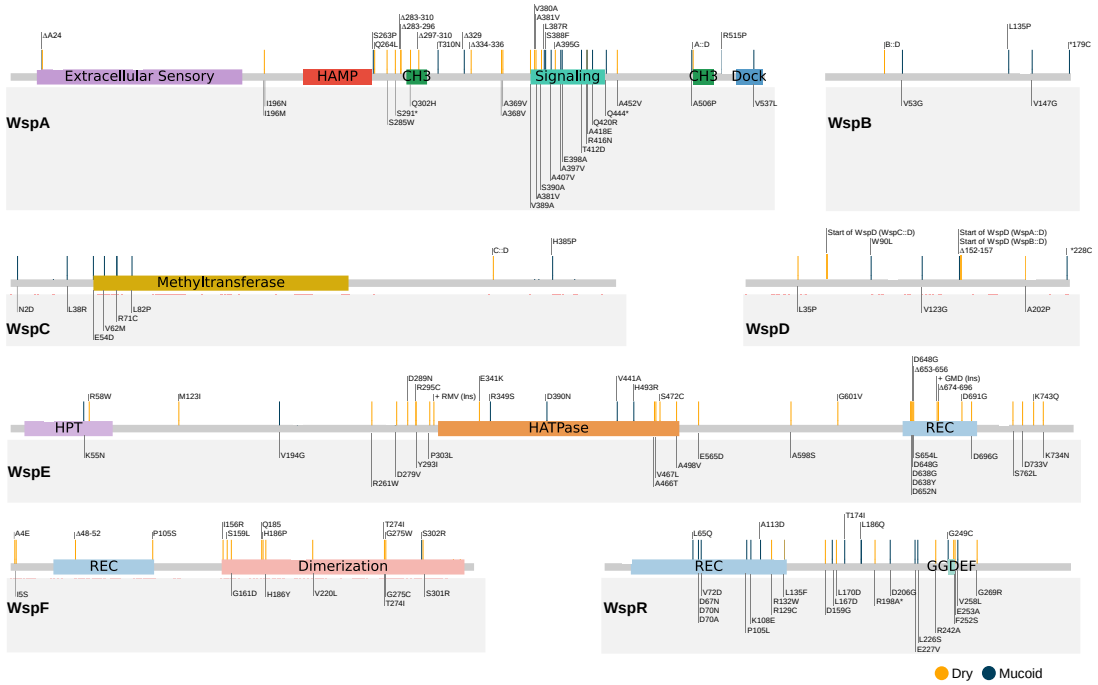

Figure 2. Alignment of our missense and in-frame deletion mutation data with previously annotated mutations in the Wsp system. Individual Wsp proteins are shown with their functional domains that were derived from CDD (NCBI), Prosite, or homology to the *E. coli* chemotaxis system (HAMP = transmembrane relay domain, CH_3 = methylation site, HPT = histidine phospho-transfer domain, HATPase = histidine kinase ATP binding domain, and REC = phosphoreceiver domain). Only the missense and in-frame mutations identified in this study are shown above each protein and they are mapped to the consensus sequence of each Wsp protein (17). Previously annotated mutations (17) are shown within the gray box below each protein. Mutations indicated within the gray box are annotated to represent specific residues positions that were affected in the respective protein sequence of a given organism, but the grey horizontal bars indicate their actual positions within the consensus sequence. Therefore, the horizontal bar locations of the mutations identified in this study are directly comparable to previously identified mutations through the consensus sequence. Mutations that stimulate c-di-GMP production are indicated by orange horizontal bars and those that reduce c-di-GMP production are indicated by blue horizontal bars.

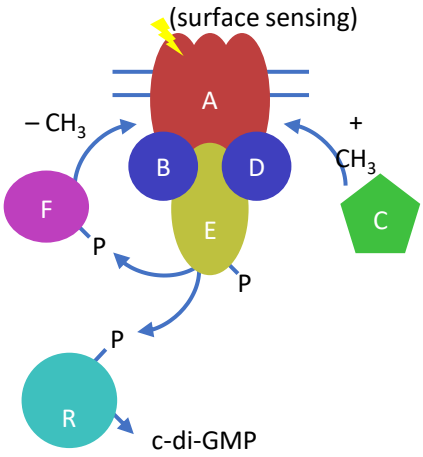

Figure 3. Functional model of the Wsp signal transduction system. The Wsp system in *P. aeruginosa* responds to surface contact to ultimately produce c-di-GMP. (CH3 = methyl group, P= phosphoryl group). Homology with the chemotaxis system predicts that once WspA is stimulated by surface-contact, it undergoes a conformational change to expose cytosolic methylation helices that are necessary for signal transduction (29). The methyl-transferase WspC is then predicted to dock at the 5' tail of WspA and methylate the WspA trimer-of-dimers complex (56). The signal is then relayed through the coupling proteins WspB and WspD, and subsequently to WspE, which functions as a histidine kinase (57). WspE phosphorylates the DGC WspR to stimulate c-di-GMP production (58). Simultaneously, WspE phosphorylates the methyl-esterase WspF, which de-methylates WspA and terminates the signaling cascade (26). Significant work has been carried out to characterize the biochemical functions of WspE and WspR in particular, and WspE is a common mutational target in a clinical setting (17). More recently, studies have begun to explore the functional role of WspA during signal activation and subcellular localization, revealing that both properties are dependent on WspB and WspD proteins (27, 59). These studies also suggest that WspB and WspD likely possess unique functions, but they remain unresolved.

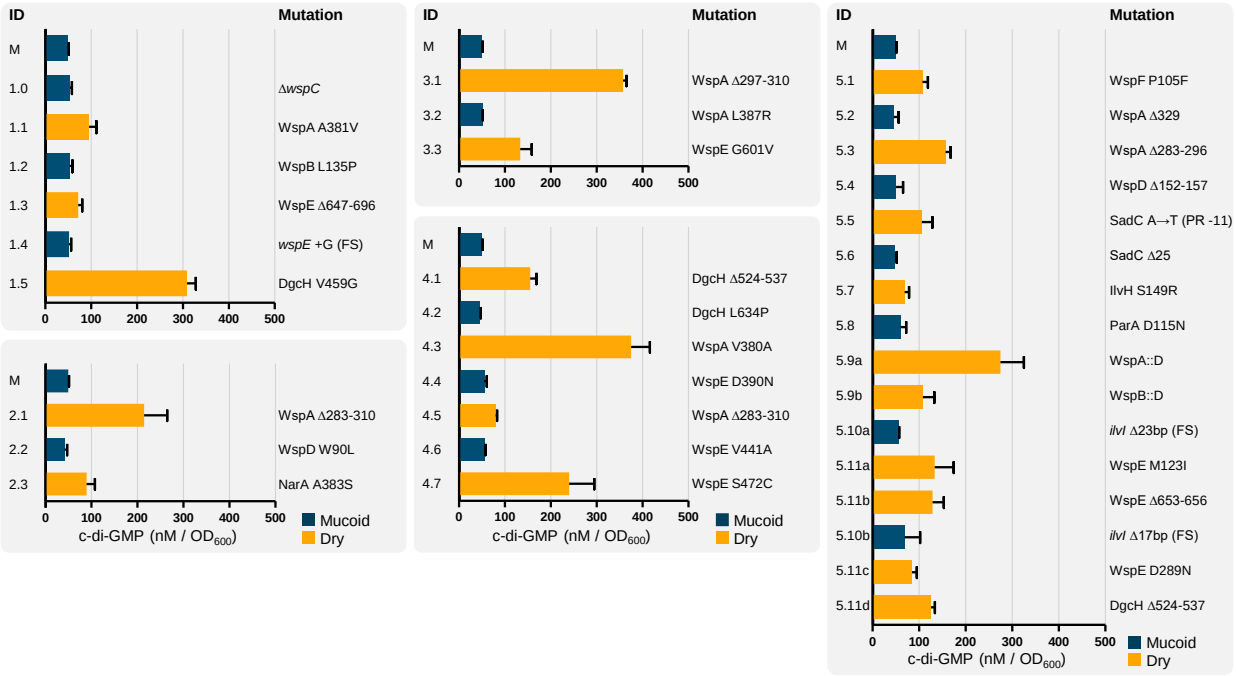

Figure 4. C-di-GMP oscillates between all M and D phenotypic transitions. C-di-GMP was quantified via LC-MS/MS and is reported as the triplicate mean ± SD. The charts capture the independently evolved strains within the five selected lineages shown in Figure 1B. D strains are shown in orange and M strains are shown in blue and their respective colony morphologies are shown in Fig. S2. The numerical IDs correspond to Table S1, and mutations reflect the affected amino acid residues, except frameshift (FS) and promoter region (PR) mutations refer to the specific nucleotides.

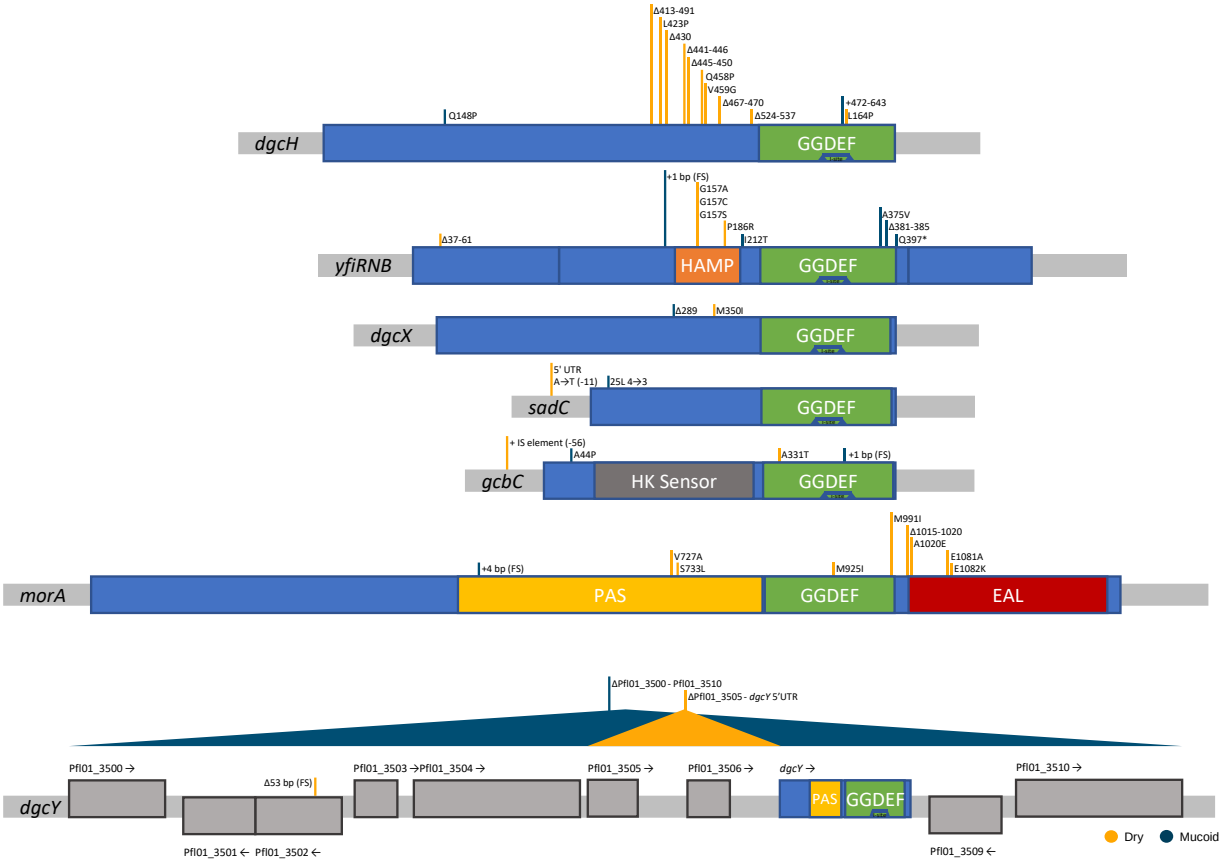

Figure 5. Alignment of our mutation data to annotated domains in known or predicted DGCs. Blue boxes represent the protein sequence and their flanking grey boxes represent untranslated regions. Each image represents a single DGC as indicated, with the exception of *yfiRNB* and *dgcY*. *YfiRNB* shows three blue boxes with each box representing YfiR, YfiN (DGC), or YfiB, respectively. *DgcY* shows a cluster of 10 genes with nine hypothetical genes of undetermined function and one bioinformatically predicted DGC (*dgcY*). Domain data were derived from CDD (NCBI): GGDEF = c-di-GMP catalytic domain, PAS = sensory signaling domain, EAL = phosphodiesterase hydrolysis domain, HAMP = transmembrane relay domain, I-site = c-di-GMP allosteric regulation site (shown inside GGDEF), HK Sensor = histidine kinase sensory domain. Mutations that stimulate c-di-GMP production are indicated by orange horizontal bars and those that reduce c-di-GMP production are indicated by blue horizontal bars.

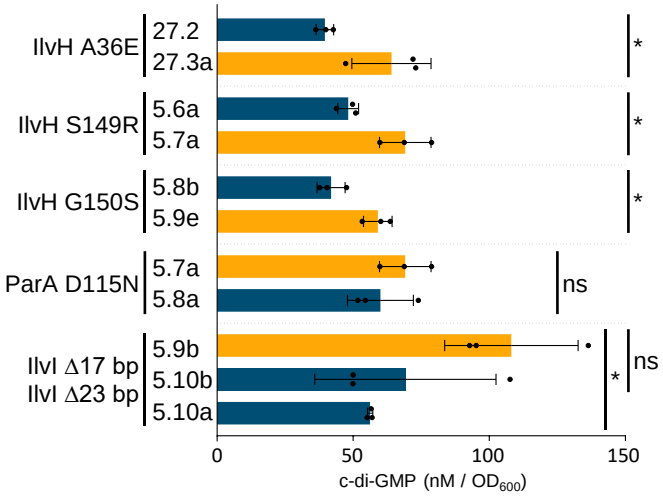

Figure 6. C-di-GMP levels fluctuate with BCAA mutations. C-di-GMP measurements in triplicate mean ± SD. Raw c-di-GMP values of each mutant and its respective parent are reported in Table S1. Causal mutation of each phenotypic shift is indicated on the left. D strains are shown in orange and M strains are shown in blue. (Student's t-test: ns = non-significant, * = $p < 0.05$).

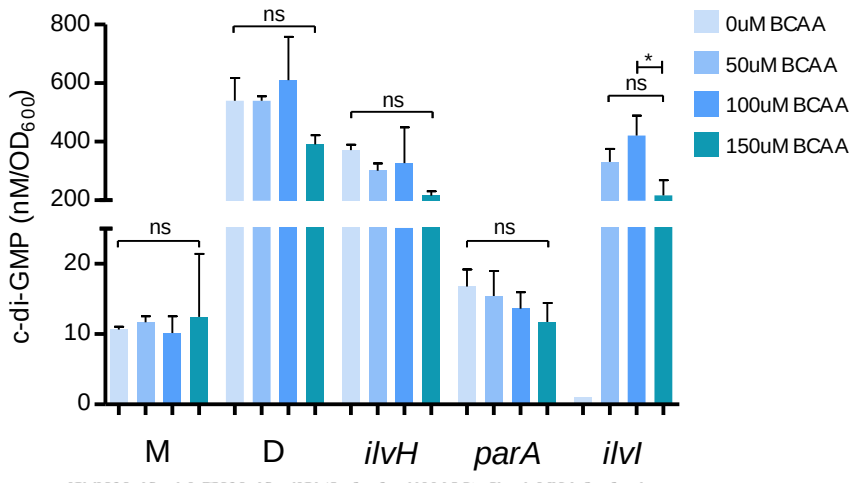

Figure 7. BCAA supplementation stimulates c-di-GMP production in a BCAA auxotroph with the M phenotype, but does not impact c-di-GMP production in non-BCAA auxotrophs with the same M phenotype. Strains were grown in the chemically defined PMM medium with 0, 50, 100, or 150 uM BCAA supplementation (valine, leucine, isoleucine). C-di-GMP was extracted and quantified via LC-MS/MS in triplicates and plotted as the mean with STD (ANOVA; Tukey's HSD Post Test: ns = non-significant, * = $p < 0.05$). M and D refer to the prototypical M and D strains in Fig. 1A. The *ilvH* mutant (D strain 5.7) produces c-di-GMP levels similar to the D strain control and the *parA* mutant (M strain 5.8) produces c-di-GMP levels similar to the M strain control. These relative patterns are consistent with the c-di-GMP quantification data reported in Fig 6 under nutrient-rich conditions. Exogenous supplementation of BCAA across all concentrations does not significantly impact c-di-GMP production. There is no data for the *ilvI* mutant at 0 uM BCAA, since this strain fails to grow in PMM unless BCAA is exogenously provided. However, the *ilvI* mutant (M strain 5.10a) produces c-di-GMP levels comparable to both D and the *ilvH* mutant (D strain 5.7) with BCAA supplementation.

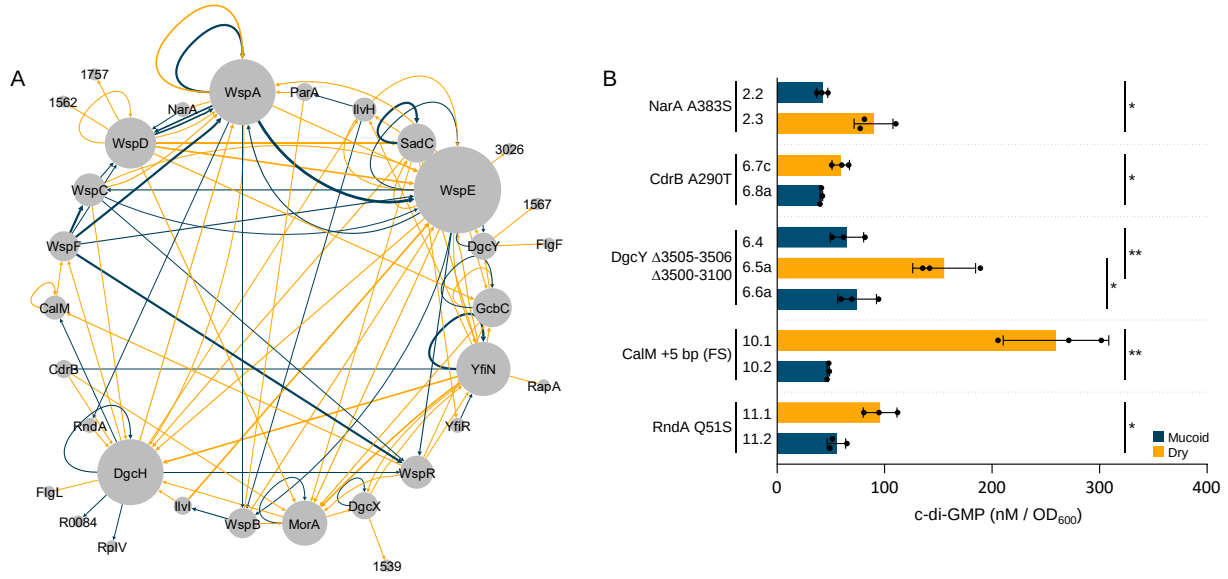

852

853 **Figure 8. A node-edge representation of 147 unique mutations across 33 lineages and c-di-GMP**

854 **quantification data of strains with mutations in proteins with significant network connectivity that are**

855 **not known to be associated with c-di-GMP modulation.** A) A node-edge plot reveals focal proteins

856 under selection. Each node represents a protein and each edge represents a relationship where one

857 mutation precedes or proceeds another. Orange edges represent M to D shifts and blue edges represent

858 D to M shifts. The relative size of a node and thickness of an edge is proportional to frequencies within

859 the dataset. Proteins that collectively form the ring represent commonly mutated targets in this study

860 and likely have a substantial role in c-di-GMP regulation. Proteins with limited connectivity fall outside

861 the main ring. B) LC-MS/MS validates that proteins with significant network connectivity, but not

862 previously associated with c-di-GMP, have a significant impact on intracellular c-di-GMP levels. C-di-

863 GMP measurements are reported as the triplicate mean ± SD. C-di-GMP values of each mutant and its

864 respective parent are summarized in Table S1 with the corresponding ID tag. D strains are shown in

865 orange and M strains are shown in blue. (Student's t-test: * = $p < 0.05$, ** = $p < 0.01$).

866 **Table 1. Reconstructing select naturally acquired mutations in both the ancestral and direct parent**

867 **strains reveal dependence on the previous mutation(s) to drive specific M-D phenotypic shifts.**

Strain ID	Strain Mutation	Mutation CDS ID	Mutant Phenotype	Parent Strain ID	Parent Strain Mutation	Ancestor ǂ	Reconstructed Mutants*	
							Parent	Ancestor
5.9a	WspA::D	Pfl01_1052::1055	dry	5.8a	ParA (D115N)	M	dry	mucoid
5.9b	WspB::D	Pfl01_1053::1055	dry	5.8a	ParA (D115N)	M	dry	mucoid
30.1	WspC::D	Pfl01_1054::1055	dry	Δ*rsmE*	Δ*rsmE*	M	dry	dry
27.3b	IlvH (A36E)	Pfl01_4787	dry	27.2	DcgH (Q148P)	M	dry	mucoid
5.7a	IlvH (S149R)	Pfl01_4787	dry	5.6a	SadC (25L 4→3)	M	dry	mucoid
5.9e	IlvH (G150S)	Pfl01_4787	dry	5.8b	YfiN (I212T)	M	dry	mucoid
5.10b	IlvI (Δ17bp)	Pfl01_4788	mucoid	5.9b	WspB::D	D	mucoid	dry
5.10a	IlvI (Δ 23bp)	Pfl01_4788	mucoid	5.9b	WspB::D	D	mucoid	dry
6.5a	DgcY (Δ3505-3506)	Pfl01_3505-3506	dry	6.4	WspE (+1bp)	M	dry	mucoid
6.6a	DgcY (Δ3500-3510)	Pfl01_3500-3510	mucoid	6.5a	DgcY (Δ3505-3506)	D	mucoid	dry
2.3	NarA (A383S)	Pfl01_3147	dry	2.2	WspD (W90L)	M	dry	mucoid
10.2	CalM (+5bp)	Pfl01_1895	mucoid	10.1	DgcH (Δ467-470)	D	mucoid	dry
11.2	RndA (Q51S)	Pfl01_2749	mucoid	11.1	WspA (A381V)	D	mucoid	dry
6.8a	CdrB (A290T)	Pfl01_0652	mucoid	6.7c	YfiN (G157C)	D	mucoid	dry

868 ǂ Ancestors are the prototype M or D strains (Fig. 1).

869 * Each mutation was reconstructed in the direct parent and the corresponding ancestor strain. WGS

870 confirmed the reconstruction of each mutation.

871 **Supplementary Information**

Figure S1

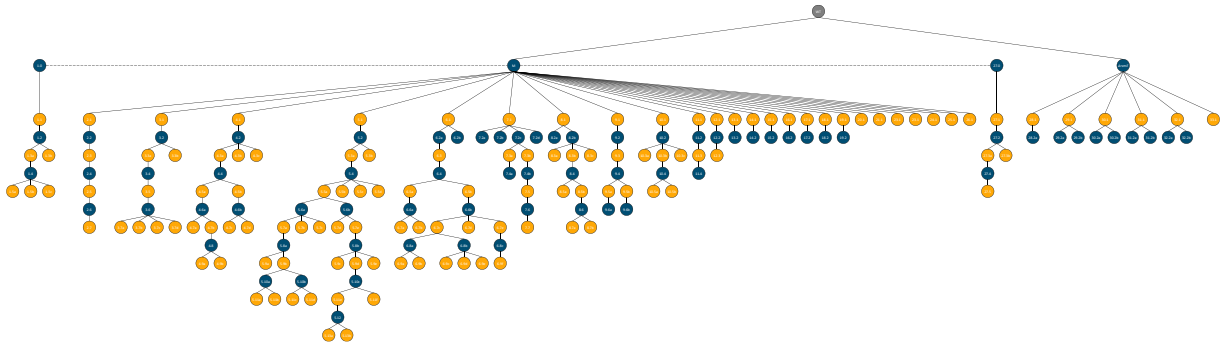

872

873 **Figure S1. Phylogeny of 191 evolved strains across 33 lineages.** Each strain is classified as either D

874 (orange) or M (blue) based on their colony morphology. Corresponding motility data, mutation data,

875 and LC-MS/MS c-di-GMP quantification data are summarized in Table S1.

Figure S2

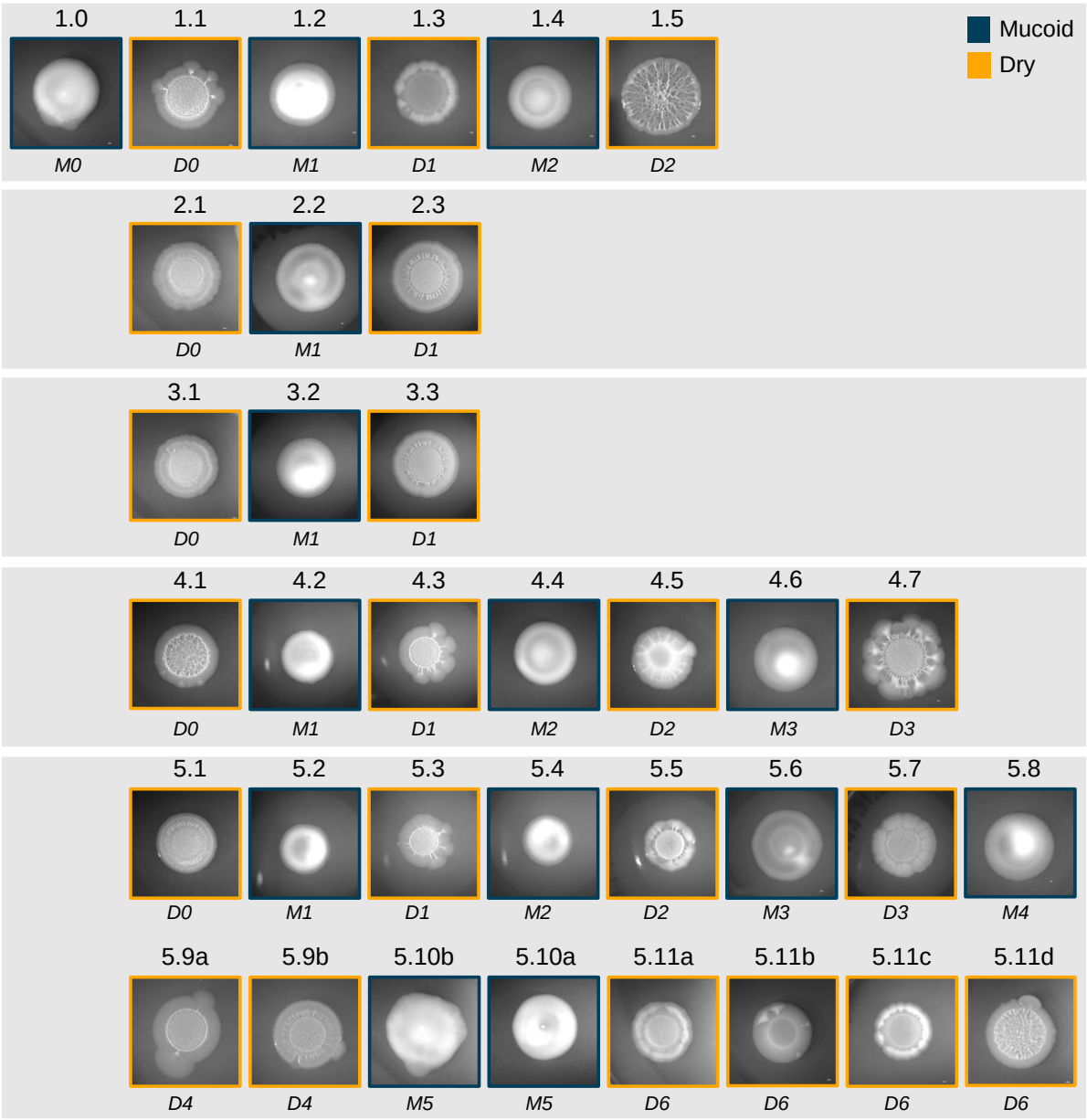

Figure S2. Colony morphologies of evolved strains depicted in Fig. 1B. Each evolved strain is classified either as M (blue) or D (orange) based on their mucoid or dry-wrinkly colony phenotypes, respectively. Motility data and LC-MS/MS c-di-GMP quantification data for each strain are reported in Table S1.

Figure S3

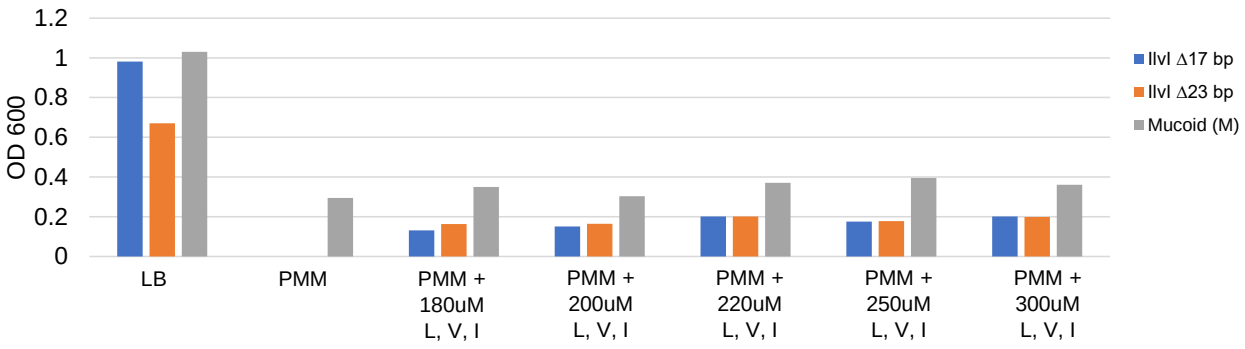

Figure S3. *ilvI* mutants require exogenous supplementation of BCAA. The ancestral M and independently isolated *ilvI* mutant strains were grown in LB (nutrient-rich medium) or PMM (minimal medium) with or without exogenous BCAA supplementation. Both *ilvI* mutants fail to grow in PMM unless supplied with BCAA (leucine (L), valine (V), and isoleucine (I)), and M does not show substantial change in growth with BCAA supplementation.

Table S1. 191 strains isolated from the parallel evolution experiment categorized by lineage.

Strain ID §	Generation §§	Motility Assay †	LC-MS/MS (nM/OD 600) ‡			Locus ***	CDS ID ***	Mutation Location (NT) ***	Consequence ***	Genotype (AA) ***	Genotype (NT) ***
			Replicate A	Replicate B	Replicate C						
WT #	WT	motile	59.23	73.16	62.21	na	na	na	na	na	na
M *	M0	motile	49.19	51.54	48.64	RsmE	Pfl01_1912 ←	2186046	Frame shift	Frame shift	Δ1 bp 126/195 nt
D **	D0	non-motile	187.52	146.52	156.37	WspC	Pfl01_1054 →	1222594	In-frame readthrough	In-frame readthrough	Δ2 bp 1269-1270/1278 nt
1.0 **	M0	motile	49.64	58.15	53.51	WspC	Pfl01_1054 →	1221330	In-frame Δ	Δ*wspC*	Δ5-1278/1278 nt
1.1	D0	non-motile	80.66	94.75	112.01	WspA	Pfl01_1052 →	1220312	Missense	A381V	GCC→GTC
1.2	M1	motile	52.28	59.70	47.26	WspB	Pfl01_1053 →	1221196	Missense	L135P	CTG→CCG
1.3a	D1	non-motile	63.54	81.09	71.31	WspE	Pfl01_1056 →	1225308	In-frame Δ	Δ674-696	Δ2029-2097/2295 nt
1.3b	D1	non-motile				WspE	Pfl01_1056 →	1225307	Duplication	673GMD 1→2	+9bp 2028/2295 nt
1.4	M2	motile	56.99	49.71	49.42	WspE	Pfl01_1056 →	1224117	Frame shift	289*	+1bp 838/2295
1.5a	D2	non-motile	290.55	328.67	307.72	DgcH	Pfl01_0050 ←	55870	Missense	V459G	GTC→GGC
1.5b	D2	non-motile				DgcH	Pfl01_0050 ←	55317	Duplication	+472-643 @ 643	+513bp 1929/2091 nt
1.5c	D2	non-motile				Pfl01_3026	Pfl01_3026 →	3463653	Missense	T242I	ACC→ATC
2.1	D0	non-motile	167.26	267.13	209.38	WspA	Pfl01_1052 →	1220020	In-frame Δ	Δ283-310	Δ850-933/1623 nt
2.2	M1	motile	47.27	41.65	36.89	WspD	Pfl01_1055 →	1222868	Missense	W90L	TGG→TTG
2.3	D1	non-motile	77.37	81.28	110.54	NarA	Pfl01_3147 →	3613968	Missense	A383S	GCC→TCC
2.4	M2	motile				WspD	Pfl01_1055 →	1223197	Nonsense	R200*	CGA→TGA
2.5	D2	non-motile				GcbC	Pfl01_4665 →/ → Pfl01_4666	5266677	5' UTR	+ Pfl01_2031-2032	+1316 +54/-56
2.6	M3	motile				WspA	Pfl01_1052 →	1219276	Nonsense	E36*	GAA→TAA
2.7	D3	non-motile				DgcH	Pfl01_0050 ←	55909	In-frame Δ	Δ441-446	Δ15bp 1323-1337/2091 nt
3.1	D0	non-motile	349.34	359.63	363.90	WspA	Pfl01_1052 →	1220059	In-frame Δ	Δ297-310	Δ889-930/1623 nt
3.2	M1	motile	49.45	51.62	51.41	WspA	Pfl01_1052 →	1220330	Missense	L387R	CTG→CGG
3.3a	D1	non-motile	127.36	112.64	160.92	WspE	Pfl01_1056 →	1225081	Missense	G601V	GGC→GTC
3.3b	D1	non-motile				WspE	Pfl01_1056 →	1224300	Missense	E341K	GAA→AAA
3.4	M2	motile				WspR	Pfl01_1058 →	1227186	Missense	L186Q	CTG→CAG
3.5	D2	non-motile				YfiN	Pfl01_0692 →	818804	Missense	G157A	GGT→GCT
3.6	M3	motile				YfiN	Pfl01_0692 →	819473	In-frame Δ	Δ381-385	Δ1139-1153/1269 nt
3.7a	D3	non-motile				DgcX	Pfl01_3550 →	4023270	Missense	M350I	ATG→ATA
3.7b	D3	non-motile				GcbC	Pfl01_4665 →/ → Pfl01_4666	5266677	5' UTR	+ Pfl01_2031-2032	+1316 +54/-56
3.7c	D3	non-motile				MorA	Pfl01_4876 →	5499015	Missense	M991I	ATG→ATA
3.7d	D3	non-motile				MorA	Pfl01_4876 →	5499101	Missense	A1020E	GCG→GAG
4.1	D0	non-motile	145.66	170.85	148.76	DgcH	Pfl01_0050 ←	55647	In-frame Δ	Δ524-537	Δ1558-1599/2091 nt
4.2	M1	motile	42.78	46.36	47.13	DgcH	Pfl01_0050 ←	55345	Missense	L634P	CTC→CCC
4.3a	D1	non-motile	392.53	328.69	404.68	WspA	Pfl01_1052 →	1220309	Missense	V380A	GTC→GCC
4.3b	D1	non-motile				WspF	Pfl01_1057 →	1226046	Missense	S159L	TCG→TTG
4.3c	D1	non-motile				WspA	Pfl01_1052 →	1220170	In-frame Δ	Δ334-336	Δ1000-1008/1623 nt
4.4	M2	motile	50.14	53.49	61.31	WspE	Pfl01_1056 →	1224447	Missense	D390N	GAC→AAC
4.5a	D2	non-motile	81.95	81.25	75.76	WspA	Pfl01_1052 →	1220020	In-frame Δ	Δ283-310	Δ850-933/1623 nt
4.5b	D2	non-motile				WspA	Pfl01_1052 →	1219961	Missense	Q264L	CAG→CTG
4.6a	M3	motile	57.50	54.72	51.88	WspE	Pfl01_1056 →	1224601	Missense	V441A	GTG→GCG
4.6b	M3	motile	54.52	56.68	55.08	WspD	Pfl01_1055 →	1223058	In-frame Δ	Δ152-157	Δ459-476/684 nt
4.7a	D3	non-motile	275.45	268.03	177.32	WspE	Pfl01_1056 →	1224693	Missense	S472C	AGT→TGT
4.7b	D3	non-motile				GcbC	Pfl01_4665 →/ → Pfl01_4666	5266677	5' UTR	+ Pfl01_2031-2032	+1316 +54/-56
4.7c	D3	non-motile				FleN	Pfl01_1562 →	1752356	Missense	T13I	ACC→ATC
4.7d	D3	non-motile				CysH	Pfl01_1757 ←	1952544	Nonsense	W51*	TGG→TGA
4.8	M4	motile				GcbC	Pfl01_4666 →	5268046	Frame shift	Frame shift	+1bp 1314/1506 nt
4.9a	D4	non-motile				DgcY	Pfl01_3502	3982758	Frame shift	Frame shift	Δ502-555/672 nt
4.9b	D4	non-motile				MorA	Pfl01_4876 →	5498817	Missense	M925I	ATG→ATC
5.1	D0	non-motile	106.41	95.85	119.21	WspF	Pfl01_1057 →	1225883	Missense	P105S	CCG→TCG
5.2	M1	motile	39.11	39.97	57.53	WspA	Pfl01_1052 →	1220156	In-frame Δ	Δ329	Δ986-988/1623 nt
5.3a	D1	non-motile	158.40	145.92	166.92	WspA	Pfl01_1052 →	1220017	In-frame Δ	Δ283-296	Δ847-888/1623 nt
5.3b	D1	non-motile				WspA	Pfl01_1052 →	1220020	In-frame Δ	Δ283-310	Δ850-933/1623 nt
5.4	M2	motile	40.20	67.63	44.65	WspD	Pfl01_1055 →	1223058	In-frame Δ	Δ152-157	Δ459-476/684 nt
5.5a	D2	non-motile	131.86	92.83	93.92	SadC	Pfl01_4451 ←	5013023	5' UTR	5' UTR	A→T (-11)
5.5b	D2	non-motile				SadC	Pfl01_4451 ←	5013023	5' UTR	5' UTR	A→C (-11)
5.5c	D2	non-motile				SadC	Pfl01_4451 ←	5013023	5' UTR	5' UTR	A→C (-11)
5.5d	D2	non-motile				WspE	Pfl01_1056 →	1224211	Duplication	308RMV 1→2	+9bp 932/2295
5.6a	M3	motile	49.79	50.94	43.86	SadC	Pfl01_4451 ←	5012937	In-frame Δ	25L 4→3	Δ74-76/1107 nt
5.6b	M3	motile				SadC	Pfl01_4451 ←	5012937	In-frame Δ	25L 4→3	Δ74-76/1107 nt
5.7a	D3	non-motile	68.79	59.84	78.79	IlvH	Pfl01_4787 ←	5402643	Missense	S149R	AGT→AGG
5.7b	D3	non-motile				DgcH	Pfl01_0050 ←	55647	In-frame Δ	Δ524-537	Δ1558-1599/2091 nt
5.7c	D3	non-motile				WspE	Pfl01_1056 →	1225351	Missense	D691G	GAC→GGC
5.7d	D3	non-motile				WspE	Pfl01_1056 →	1224324	Missense	R349S	CGC→AGC
5.7e	D3	non-motile				YfiN	Pfl01_0692 →	818804	Missense	G157A	GGT→GCT
5.8a	M4	motile	54.44	51.70	73.94	ParA	Pfl01_0730 →	858438	Missense	D115N	GAT→AAT

5.8b	M4	motile	47.61	37.67	40.41	YfiN	Pfl01_0692 →	818969	Missense	I212T	ATT→ACT
5.9a	D4	non-motile	329.69	230.96	263.57	WspA	Pfl01_1052 →	1220649	In-frame Δ	wspA::D	Δ2421 bp
5.9b	D4	non-motile	92.77	95.21	136.41	WspB	Pfl01_1053 →	1220923	In-frame Δ	wspB::D	Δ1840 bp
5.9c	D4	non-motile				WspE	Pfl01_1056 →	1223451	Missense	R58W	CGG→TGG
5.9d	D4	non-motile				WspE	Pfl01_1056 →	1223648	Missense	M123I	ATG→ATA
5.9e	D4	non-motile	53.36	63.66	60.18	IlvH	Pfl01_4787 ←	5402642	Missense	G150S	GGC→AGC
5.10a	M5	motile	56.96	56.62	55.12	IlvI	Pfl01_4788 ←	5403629	Frame shift	Frame shift	Δ23bp 1166-1188/1725 nt
5.10b	M5	motile	49.96	49.89	107.61	IlvI	Pfl01_4788 ←	5403629	Frame shift	Frame shift	Δ17bp 1172-1188/1725 nt
5.10c	M5	motile				WspR	Pfl01_1058 →	1227150	Missense	T174I	ACC→ATC
5.11a	D5	non-motile	110.47	109.78	180.81	WspE	Pfl01_1056 →	1223648	Missense	M123I	ATG→ATA
5.11b	D5	non-motile	104.23	129.78	152.89	WspE	Pfl01_1056 →	1225239	In-frame Δ	Δ653-656	Δ12bp 1960-1971/2295 nt
5.11c	D5	non-motile	81.07	77.14	96.70	WspE	Pfl01_1056 →	1224144	Missense	D289N	GAC→AAC
5.11d	D5	non-motile	128.07	115.76	132.55	DgcH	Pfl01_0050 ←	55647	In-frame Δ	Δ524-537	Δ1558-1599/2091 nt
5.11e	D5	non-motile				GcbC	Pfl01_4665 →/ → Pfl01_4666	5266677	5' UTR	+ Pfl01_2031-2032	+1316 +54/-56
5.11f	D5	non-motile				MorA	Pfl01_4876 →	5499284	Missense	E1081A	GAA→GCA
5.12	M6	motile				GcbC	Pfl01_4666 →	5266862	Missense	A44P	GCC→CCC
5.13a	D6	non-motile				MorA	Pfl01_4876 →	5499088	In-frame Δ	Δ1015-1020	Δ15bp 3046-3060/3849 nt
5.13b	D6	non-motile				GcbC	Pfl01_4666 →	5267723	Missense	A331T	GCC→ACC
6.1	D0	non-motile				WspF	Pfl01_1057 →	1226544	Frame shift	KI325R*	Δ974/1011 nt
6.2a	M1	motile				WspA	Pfl01_1052 →	1219239	Duplication	L23 2→3	+3bp 69/1623
6.2b	M1	motile				WspR	Pfl01_1058 →	1227374	Missense	G249C	GGC→TGC
6.3	D1	non-motile				WspA	Pfl01_1052 →	1219239	Duplication	L24 3→2	-3bp 69/1623
6.4	M2	motile	51.19	81.77	61.87	WspE	Pfl01_1056 →	1225435	Frame shift	748*	+1bp 2156/2295 nt
6.5a	D2	non-motile	189.04	141.94	135.43	DgcY	[Pfl01_3505]–Pfl01_3506	3985701	In-frame Δ	124* Δ5' UTR 3508	Δ3505,Δ3506,Δ3508 5'UTR
6.5b	D2	non-motile				SadC	Pfl01_4451 ←	5013023	5' UTR	5' UTR	A→C (-11)
6.6a	M3	motile	69.41	59.49	94.44	DgcY	[Pfl01_3500]–Pfl01_3510	3981080	In-frame Δ	Δ10 proteins	Δ3500-3510
6.6b	M3	motile				SadC	Pfl01_4451 ←	5012937	In-frame Δ	25L 4→3	Δ74-76/1107 nt
6.7a	D3	non-motile				CheB	Pfl01_1567	1758645	Frame shift	Frame shift	Δ1bp 1061/1137 nt
6.7b	D3	non-motile				FlgF	Pfl01_1501 →	1680303	Frame shift	Frame shift	Δ14bp 138-151/741 nt
6.7c	D3	non-motile	66.67	50.69	60.25	YfiN	Pfl01_0692 →	818803	Missense	G157C	GGT→TGT
6.7d	D3	non-motile				DgcH	Pfl01_0050 ←	55952	Frame shift	Δ430	Δ1292-1294/2091 nt
6.7e	D3	non-motile				YfiR	Pfl01_0691 →	817876	In-frame Δ	Δ37-61	Δ114-188/576 nt
6.8a	M4	motile	41.34	42.22	39.91	CdrB	Pfl01_0652 ←	763630	Missense	A290T	GCC→ACC
6.8b	M4	motile				YfiN	Pfl01_0692 →	819458	Missense	A375V	GCG→GTG
6.8c	M4	motile				YfiN	Pfl01_0692 →	818709	Frame shift	Frame shift	+1bp 375/1269 nt
6.9a	D4	non-motile				DgcH	Pfl01_0050 ←	55978	Missense	L423P	CTC→CCC
6.9b	D4	non-motile				MorA	Pfl01_4876 →	5499015	Missense	M991I	ATG→ATA
6.9c	D4	non-motile				MorA	Pfl01_4876 →	5499015	Missense	M991I	ATG→ATT
6.9d	D4	non-motile				DgcH	Pfl01_0050 ←	55647	In-frame Δ	Δ524-537	Δ1558-1599/2091 nt
6.9e	D4	non-motile				GcbC	Pfl01_4665 →/ → Pfl01_4666	5266677	5' UTR	+ Pfl01_2031-2032	+1316 +54/-56
6.9f	D4	non-motile				RapA	Pfl01_1678 ←	1873535	Missense	S317A	TCG→GCG
7.1	D0	non-motile	187.52	146.52	156.37	WspC	Pfl01_1054 →	1222594	In-frame Δ	*wspC::D*	Δ1269-1270/1278 nt
7.2a	M1	motile				WspE	Pfl01_1056 →	1223360	Frame shift	156*	+1bp 81/2295 nt
7.2b	M1	motile				WspR	Pfl01_1058 →	1227186	Frame shift	205*	Δ1bp 557/1002 nt
7.2c	M1	motile				WspD	Pfl01_1055 →	1223058	In-frame Δ	Δ152-157	Δ459-476/684 nt
7.2d	M1	motile				WspD	Pfl01_1055 →	1223058	In-frame Δ	Δ152-157	Δ459-476/684 nt
7.3a	D1	non-motile				WspE	Pfl01_1056 →	1223648	Missense	M123I	ATG→ATA
7.3b	D1	non-motile				WspE	Pfl01_1056 →	1224162	Missense	R295C	CGC→TGC
7.4a	M2	motile				WspD	Pfl01_1055 →	1222912	Nonsense	Q105*	CAG→TAG
7.4b	M2	motile				WspE	Pfl01_1056 →	1224637	Missense	H453R	CAC→CGC
7.5	D2	non-motile				SadC	Pfl01_4451 ←	5013023	5' UTR	5' UTR	A→C (-11)
7.6	M3	motile				SadC	Pfl01_4451 ←	5012937	In-frame Δ	25L 4→3	Δ74-76/1107 nt
7.7	D3	non-motile				MorA	Pfl01_4876 →	5498240	Missense	S733L	TCG→TTG
8.1	D0	non-motile				WspF	Pfl01_1057 →	1226036	Missense	I156R	ATC→CGA
8.2a	M1	motile				WspC	Pfl01_1054 →	1222439	Nonsense	Q372*	CAG→TAG
8.2b	M1	motile				WspD	Pfl01_1055 →	1223283	Missense	*228C (WspD::E)	TGA→TGC
8.3a	D1	non-motile				GcbC	Pfl01_4665 →/ → Pfl01_4666	5266677	5' UTR	+ Pfl01_2031-2032	+1316 +54/-56
8.3b	D1	non-motile				MorA	Pfl01_4876 →	5499015	Missense	M991I	ATG→ATA
8.3c	D1	non-motile				MorA	Pfl01_4876 →	5499286	Missense	E1082K	GAA→AAA
8.4	M2	motile				MorA	Pfl01_4876 →	5497033	Frame shift	487*	+4bp 991/3849nt
8.5a	D2	non-motile				DgcH	Pfl01_0050 ←	55773	In-frame Δ	Δ413-491	Δ1237-1473/2091 nt
8.5b	D2	non-motile				DgcX	Pfl01_3550 →	4023270	Missense	M350I	ATG→ATA
8.6	M3	motile				DgcX	Pfl01_3550 →	4023085	In-frame Δ	Δ289	Δ3bp 865-867/1680 nt
8.7a	D3	non-motile				YfiN	Pfl01_0692 →	818891	Missense	P186R	CCG→CGG
8.7b	D3	non-motile				FliI	Pfl01_1539 →	1729003	Frame shift	Frame shift	+1bp 1015/1359 nt
9.1	D0	non-motile				WspF	Pfl01_1057 →	1226393	Missense	G275W	GGG→TGG
9.2	M1	motile				WspE	Pfl01_1056 →	1223361	Frame shift	38*	Δ82-127/2295 nt
9.3	D1	non-motile				YfiN	Pfl01_0692 →	818803	Missense	G157S	GGT→AGT

9.4	M2	motile				YfiN	Pfl01_0692 →	819523	Nonsense	Q397*	CAA→TAA
9.5a	D2	non-motile				DgcH	Pfl01_0050 ←	55896	In-frame Δ	Δ445-450	Δ1333-1350/2091 nt
9.5b	D2	non-motile				DgcH	Pfl01_0050 ←	55647	In-frame Δ	Δ524-537	Δ1558-1599/2091 nt
9.6a	M3	motile				tRNA	Pfl01_R0084 ←	5451395	5' UTR	5' UTR	G→T 49/77nt
9.6b	M3	motile				RplV	Pfl01_5074 ←	5702436	Missense	A43T	GCC→ACC
10.1	D0	non-motile	301.71	271.29	205.50	DgcH	Pfl01_0050 ←	55835	In-frame Δ	Δ467-470	Δ1400-1411/2091 nt
10.2	M1	motile	48.63	48.06	46.64	CalM	Pfl01_1895 →	2166348	Frame shift	Frame shift	+5bp 1685/2652 nt
10.3a	D1	non-motile				CalM	Pfl01_1895 →	2166348	In-frame Δ	In-frame Δ	-5bp 1685/2652 nt
10.3b	D1	non-motile				WspF	Pfl01_1057 →	1226204	Nonsense	E212*	GAA→TAA
10.3c	D1	non-motile				CalM	Pfl01_1895 →	2166348	In-frame Δ	In-frame Δ	-5bp 1685/2652 nt
10.4	M2	motile				WspR	Pfl01_1058 →	1226823	Missense	L65Q	CTG→CAG
10.5	D2	non-motile				CalM	Pfl01_1895 →	2166348	In-frame Δ	In-frame Δ	-5bp 1685/2652 nt
11.1	D0	non-motile	80.66	94.75	112.01	WspA	Pfl01_1052 →	1220312	Missense	A381V	GCC→GTC
11.2	M1	motile	49.17	51.38	65.08	RndA	Pfl01_2749 ←	3170622	Nonsense	Q51*	CAG→TAG
11.3	D1	non-motile	147.33	132.67	152.43	DgcH	Pfl01_0050 ←	55647	In-frame Δ	Δ524-537	Δ1558-1599/2091 nt
11.4	M2	motile	43.58	37.94	43.96	WspR	Pfl01_1058 →	1226967	Missense	A113D	GCC→GAC
12.1	D0	non-motile				WspE	Pfl01_1056 →	1225222	Missense	D648G	GAC→GGC
12.2	M1	motile				WspC	Pfl01_1054 →	1222526	Frame shift	421*	Δ1201-1202/1278 nt
12.3	D1	non-motile				WspA	Pfl01_1052 →	1220020	In-frame Δ	Δ283-310	Δ850-933/1623 nt
13.1	D0	non-motile				WspF	Pfl01_1057 →	1225581	Missense	A4E	GCA→GAA
13.2	M1	motile				WspC	Pfl01_1054 →	1222479	Missense	H385P	CAC→CCC
14.1	D0	non-motile				WspF	Pfl01_1057 →	1226127	Missense	H186P	CAT→CCT
14.2	M1	motile				WspA	Pfl01_1052 →	1220333	Missense	S388F	TCC→TTC
15.1	D0	non-motile				WspE	Pfl01_1056 →	1225307	Duplication	673GMD 1→2	+9bp 2028/2295 nt
15.2	M1	motile				WspF	Pfl01_1057 →	1226474	Missense	S302R	AGT→CGT
16.1	D0	non-motile				WspF	Pfl01_1057 →	1225883	Missense	P105S	CCG→TCG
16.2	M1	motile				WspC	Pfl01_1054 →	1221551	Nonsense	E76*	GAA→TAA
17.1	D0	non-motile				WspF	Pfl01_1057 →	1226391	Missense	T274I	ACA→ATA
17.2	M1	motile				WspA	Pfl01_1052 →	1219453	Nonsense	Q95*	CAG→TAG
18.1	D0	non-motile				WspF	Pfl01_1057 →	1225721	In-frame Δ	Δ48-52	Δ151-165/1011 nt
18.2	M1	motile				WspR	Pfl01_1058 →	1226688	Nonsense	L20*	TTG→TAG
19.1	D0	non-motile				WspA	Pfl01_1052 →	1220020	In-frame Δ	Δ283-310	Δ850-933/1623 nt
19.2	M1	motile				WspE	Pfl01_1056 →	1223907	Frame shift	Frame shift	-1 bp 628/2295
20	D0	non-motile				WspF	Pfl01_1057 →	1226559	Nonsense	L330*	TTG→TAG
21	D0	non-motile				WspF	Pfl01_1057 →	1225721	In-frame Δ	Δ48-52	Δ151-165/1011 nt
22	D0	non-motile				WspA	Pfl01_1052 →	1220020	In-frame Δ	Δ283-310	Δ850-933/1623 nt
23	D0	non-motile				WspF	Pfl01_1057 →	1225883	Missense	P105S	CCG→TCG
24	D0	non-motile				MorA	Pfl01_4876 →	5499286	Missense	E1082K	GAA→AAA
25	D0	non-motile				WspE	Pfl01_1056 →	1224324	Missense	R349S	CGC→AGC
26	D0	non-motile				MorA	Pfl01_4876 →	5498817	Missense	M925I	ATG→ATA
27.0 **	M0	motile				WspC	Pfl01_1054 →	1221330	In-frame Δ	Δ*wspCD*	Δ1954/1954 nt
27.1	D0	non-motile				DgcH	Pfl01_0050 ←	55873	Missense	Q458P	CAG→CCG
27.2	M1	motile	42.70	39.96	36.29	DgcH	Pfl01_0050 ←	56803	Missense	Q148P	CAG→CCG
27.3a	D1	non-motile	47.26	71.96	72.99	IlvH	Pfl01_4787 ←	5402983	Missense	A36E	GCG→GAG
27.3b	D1	non-motile				FlgL	Pfl01_1507 ←	1687852	Frame shift	326*	Δ1bp 866/1572 nt
27.4	M2	motile				WspB	Pfl01_1053 →	1221329	Missense	*179C (WspB+)	TGA→TGC
27.5	D2	non-motile				MorA	Pfl01_4876 →	5498222	Missense	V727A	GTA→GCA
ΔrsmE *	M0	motile	61.11	61.63	60.13	RsmE	Pfl01_1912 ←	2185977	In-frame Δ	Δ*rsmE*	Δ1-195/195 nt
28.1	D0	non-motile				WspA	Pfl01_1052 →	1220020	In-frame Δ	Δ283-310	Δ850-933/1623 nt
28.2	M1	motile				WspA	Pfl01_1052 →	1220716	Nonsense	Q516*	CAG→TAG
29.1	D0	non-motile				WspE	Pfl01_1056 →	1225506	Missense	K743Q	AAG→CAG
29.2a	M1	motile				WspC	Pfl01_1054 →	1221416	Frame shift	51*	+ 19bp 91/1278 nt
29.2b	M1	motile				WspA	Pfl01_1052 →	1219453	Nonsense	Q95*	CAG→TAG
30.1	D0	non-motile				WspF	Pfl01_1057 →	1226123	Nonsense	Q185*	CAG→TAG
30.2a	M1	motile				WspR	Pfl01_1058 →	1227012	Frame shift	138*	Δ1bp 383/1002 nt
30.2b	M1	motile				WspC	Pfl01_1054 →	1222448	Frame shift	389*	Δ1bp 1123/1278 nt
31.1	D0	non-motile				WspC	Pfl01_1054 →	1222342	In-frame Δ	WspC::D	Δ305bp WspC:WspD
31.2a	M1	motile				WspA	Pfl01_1052 →	1220714	Missense	R515P	CGT→CCT
31.2b	M1	motile				WspA	Pfl01_1052 →	1220099	Missense	T310N	ACC→AAC
32.1	D0	non-motile				WspE	Pfl01_1056 →	1225223	Missense	D648G	GAC→GAA
32.2a	M1	motile				WspA	Pfl01_1052 →	1219957	Missense	S263P	TCC→CCC
32.2b	M1	motile				WspB	Pfl01_1053 →	1221235	Nonsense	W148*	TGG→TAG
33.1	D0	non-motile	86.13	60.82	85.85	WspF	Pfl01_1057 →	1225721	In-frame Δ	Δ48-52	Δ151-165/1011 nt

887 § Relationships of the lineages presented here are visualized in Fig. S1. Strain IDs correspond to variant calling files found in 'Table S1 - Source Data 1' that

888 provides evidence for each reported mutation. All strains were generated in this experiment unless otherwise noted or stated here: *(60); ** (24); # (50). M and

889 D served as the prototype ancestral strains throughout this study.

890 §§ Generation refers to an individual strain's evolutionary distance from WT where the following sequence represents the accumulation of mutations at each

891 generation: WT, M0, D0, M1, D1, … M6, D6.

892 † Determined by stab-motility assays.

893 ‡ Select strains were chosen for LC-MS/MS c-di-GMP quantification conducted in triplicate.

894 *** Locus, CDS, and Mutation Location (NT) were extracted from GenBank reference CP000094 unless otherwise stated. CDS: → (+ strand), ← (- strand), /

895 (intergenic space). Genotype (AA/NT) was reported by BreSeq during variant analysis. Consequence describes the nature of mutation.

Table S2. Node-edge plot data matrix.

Source	Target	Attribute	Count
CdrB	DgcH	D	1
CdrB	MorA	D	1
ParA	WspA	D	1
ParA	WspB	D	1
CalM	CalM	D	2
CalM	WspF	D	1
RndA	DgcH	D	1
NarA	WspD	M	1
DgcY	Pfl01_1567	D	1
DgcY	FlgF	D	1
DgcY	DgcY	M	1
DgcX	Pfl01_1539	D	1
DgcX	YfiN	D	1
DgcX	DgcX	M	1
SadC	DgcH	D	2
SadC	IlvH	D	1
SadC	MorA	D	1
SadC	WspE	D	2
SadC	YfiN	D	2
SadC	YfiR	D	1
SadC	SadC	M	4
DgcH	FlgL	D	1
DgcH	IlvH	D	1
DgcH	WspA	D	2
DgcH	WspF	D	1
DgcH	CalM	M	1
DgcH	DgcH	M	2
DgcH	R0084	M	1
DgcH	RplV	M	1
DgcH	WspR	M	1
GcbC	DgcY	D	1
GcbC	GcbC	D	1
GcbC	MorA	D	2
GcbC	GcbC	M	1
IlvH	ParA	M	1
IlvH	WspB	M	1
IlvI	DgcH	D	1
IlvI	WspE	D	3
MorA	DgcX	D	1
MorA	DgcH	D	1
MorA	MorA	M	1
RsmE	DgcH	D	2
RsmE	WspA	D	4
RsmE	WspD	D	1
RsmE	WspE	D	2
RsmE	WspF	D	15
RsmE	WspD	M	1
WspA	NarA	D	1
WspA	DgcH	D	1
WspA	WspA	D	3
WspA	WspE	D	2
WspA	RndA	M	1
WspA	WspA	M	4
WspA	WspB	M	1
WspA	WspD	M	3
WspA	WspE	M	5
WspB	MorA	D	1
WspB	WspE	D	2
WspB	IlvI	M	2
WspC	DgcH	D	1
WspC	WspA	D	2
WspC	WspE	D	1
WspC	WspD	M	2
WspC	WspE	M	1
WspC	WspR	M	1
WspD	Pfl01_1562	D	1
WspD	Pfl01_1757	D	1
WspD	SadC	D	3
WspD	GcbC	D	2
WspD	MorA	D	2
WspD	WspA	D	1
WspD	WspD	D	1
WspD	WspE	D	3
WspD	WspA	M	3
WspE	Pfl01_3026	D	1
WspE	DgcY	D	1
WspE	SadC	D	2
WspE	DgcH	D	2
WspE	GcbC	D	1
WspE	MorA	D	2
WspE	WspA	D	2
WspE	WspE	D	1
WspE	YfiN	D	1
WspE	WspA	M	2
WspE	WspB	M	1
WspE	WspC	M	2
WspE	WspE	M	2
WspE	WspR	M	2
WspF	WspA	M	4
WspF	WspC	M	4
WspF	WspD	M	1
WspF	WspE	M	2
WspF	WspR	M	4
WspR	CalM	D	2
WspR	GcbC	D	1
WspR	MorA	D	1
WspR	YfiN	D	1
YfiN	DgcX	D	1
YfiN	DgcH	D	3
YfiN	GcbC	D	2
YfiN	IlvH	D	1
YfiN	MorA	D	3
YfiN	RapA	D	1
YfiN	WspE	D	2
YfiN	CdrB	M	1
YfiN	YfiN	M	4
YfiR	YfiN	M	1

* Values are reported in to-from format with source indicating the mutation a parent strain carries, target indicating the mutation a daughter cell carries, attribute indicating if said daughter cell's mutation resulted in the M or D phenotype, and count indicating the frequency of the pattern in the dataset.

901 **Table S3. Description of PCR primers used to reconstruct mutations.**

Target mutation	Forward Primer Sequence	Reverse Primer Sequence
WspA::D	ATCTGGTGAACGCCAAACT	TGACCAGGCAATCTTCCATC
WspB::D	CCACGTATGACATCGAACAGA	CTGTCGAGATCGAGCAGTTC
WspC::D	TGCCGAGAACGAAGGTTA	CTGTCGAGATCGAGCAGTTC
IlvH (A36E)	CAAGACGGAGCGTACCTAATC	AACGGTAGCCGAACCTTTAC
IlvH (S149R)	CAAGACGGAGCGTACCTAATC	AACGGTAGCCGAACCTTTAC
IlvH (G150S)	CAAGACGGAGCGTACCTAATC	AACGGTAGCCGAACCTTTAC
IlvI (Δ17bp)	AGGGAAGCTCAAAGCGATAC	AACCTGCCGGTTACCAATAC
IlvI (Δ 23bp)	AGGGAAGCTCAAAGCGATAC	AACCTGCCGGTTACCAATAC
DgcY (Δ3505-3506)	ATGGCTAAGCCCAGTTACACA	TGAAGCCGTTGAGATCGATA
DgcY (Δ3500-3510)	ATCGTTAGGGCGCTATCAATAC	TTGCATCGAGCAGGGTTTTC
NarA (A383S)	CATTTACACCTCGGGAGATGAC	CGACAGCGCATTGAAGAAAC
CalM (+5bp)	CTGCTGACCAATCCAATCCT	AAGTCATCGTCTGCCAACTC
RndA (Q51S)	TTGTTCACTCATCGCCTACTG	CGACCAGCGTTCCGATAAA
CdrB (A290T)	CGTTATCAACAGGACGGCTATC	GCTTGAGTTCCAGACCGTTATT
ilvH external check	CGCACTCCTACATGGAATCA	CAGCTACATCGGTCACTTTCA
ilvI external check	AAGCCAAACTGCGTTCCTA	TTCATCTGGATACTGCCTTCAC

902